JOURNAL OF PROPULSION AND POWER
Vol. 14, No. 5, September–October 1998

Pulsed Plasma Thruster

R. L. Burton*
University of Illinois at Urbana–Champaign, Urbana, Illinois 61801
and
P. J. Turchi†
Ohio State University, Columbus, Ohio 43210

The 35-year history of the development and application of the pulsed plasma thruster (PPT) is reviewed. The PPT operates by creating a pulsed, high-current discharge across the exposed surface of a solid insulator, such as a Teflon® bar. The arc discharge ablates material from this surface, thereby providing propellant that is ionized, heated, and accelerated to high speed. Typically, the current pulse lasts for a few microseconds, driven by a capacitor that is charged and discharged approximately once per second. Exhaust speeds range from 3 to 50 km/s, depending on the details of the PPT design. We review the basic physics and types of PPTs, and discuss the performance of flight and laboratory versions, with special attention to velocity and plume measurements. We also present the status of PPT theory and modeling, with emphasis on mass evolution and plasma acceleration, and describe recent variations on PPT operation, laboratory thrust measurement techniques, and the separate components of PPT efficiency.

I. Introduction

ON Nov. 30, 1964, the Zond 2 spacecraft was launched toward Mars from Baikonur in the Soviet Union. Several months later, radio communication was lost, and with it control of the electric propulsion system designed to provide three-axis attitude control. The Zond 2 pulsed plasma thrusters (PPTs) were the first application of electric propulsion on any spacecraft.

Other successful flight applications of the PPT followed in the United States. In 1968 a PPT on the LES-6 satellite began 10 years of service providing attitude control. In 1974 a PPT was deployed on the Synchronous Meteorological Satellite (SMS).[1] And beginning in 1981 the Navy TRANSIT navigation satellite system employed three spacecraft called the TIP/NOVA (TRANSIT Improvement Program) series, which used PPTs[2–4] for drag makeup to maintain a "drag-free" orbital position. These spacecraft accumulated a total of 28 thruster years of successful operation.

Electric propulsion is used because it provides higher exhaust speeds than available chemically, allowing significant propellant savings for several applications in space. Today, these applications include onboard propulsion for satellites that already require significant electrical power to accomplish their mission, e.g., communication. Such propulsion primarily serves stationkeeping needs,[5–8] but the capability clearly extends to orbit transfer,[9] drag compensation and formation flying,[2,10] and attitude control.[11,12] Flight experience gained in these near-Earth missions has encouraged application of electric propulsion for planetary and deep space exploration.[13,14]

Electric propulsion has also demonstrated several system advantages over chemical propulsion, leading to its selection instead of high I_{sp}. The reasons for this selection can include a longer life and less propellant leakage and toxic propellant, making electric propulsion competitive, even at comparable specific impulse.

During the past several decades, the research and development of electric propulsion has embraced a great variety of candidate systems, five of which are now flight qualified. Standard texts[15,16] provide the taxonomy of these techniques, which are loosely organized into three main categories of electrothermal, electromagnetic, and electrostatic propulsion. Of the five flight-qualified systems, two are electrothermal (resistojet and arcjet), one is electrostatic (ion thruster), and two are electromagnetic (Hall thruster and the PPT). Together, these devices cover a wide range of I_{sp} and efficiency.

This paper reviews the propulsion characteristics of the ablation-fed pulsed plasma thruster, or pulsed plasma microthruster,[7,17] generally abbreviated as PPT. Of all the various electric thruster concepts, the PPT was the first to achieve acceptance for application on space missions because of its system simplicity. Many years later the PPT was followed by the augmented hydrazine thruster, the kilowatt-level arcjet, the xenon ion engine, and the Hall or stationary plasma thruster (SPT). In contrast with the PPT, these steady-state devices achieved their optimum levels of performance after decades of development in the laboratory. Indeed, the thrust efficiency of flight models of the xenon ion engine and the SPT-100 can exceed 50%. The simplicity, robustness, short development time, and low cost of the PPT, however, allowed its selection for space-flight applications in the 1960s, despite a much lower efficiency. The PPT is thus unique in combining decades of space-qualified flight use with considerable opportunity for improved performance.

Figure 1 schematically displays a PPT in its traditional, breech-fed, rectangular form, driven by an LRC (inductance-resistance-capacitance) pulse circuit. In this arrangement (which can also be made coaxial), a solid propellant bar, usually Teflon®, fills the gap between two electrodes connected to a charged capacitor in vacuum. A spark igniter provides a small amount of initial plasma, triggering an electrical discharge across the exposed surface of the Teflon. Heat transfer from this discharge causes evaporation of propellant material, which is then accelerated by electromagnetic and pressure forces. As the propellant evaporates with each discharge, a simple spring mechanism advances the propellant bar axially into the thrust chamber, eliminating the need for a propellant tank and feed-regulation system.

Variants of the PPT include the so-called "side-fed" system (Fig. 2), which can be used in rectangular or coaxial geometry,

Received June 4, 1998; revision received June 25, 1998; accepted for publication June 29, 1998.

*Professor, Department of Aeronautical and Astronautical Engineering, 104 South Wright Street. Associate Fellow AIAA.

†Professor, Department of Aerospace Engineering, Applied Mechanics and Aviation. Associate Fellow AIAA.

but uses two propellant bars, advanced from opposite sides.[18] The coaxial arrangement (Fig. 3) was originally developed in the form of magnetoplasmadynamic (MPD) devices[19] and is now part of the PPT family.

Palumbo and Guman[20] made the systems case for the PPT following nearly 9000 h of flight operations with an early PPT called the LES-6 thruster, over a 10-year period beginning in 1968:

1) Zero warmup time, zero standby power.
2) Inert and fail-safe—no unpowered torques or forces.
3) Scaleable to performance requirements.
4) Usable on spinning or three-axis stabilized satellites.

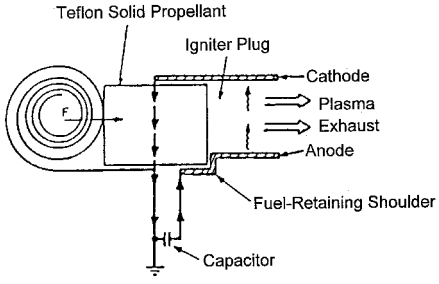

Fig. 1 Solid propellant PPT (schematic).

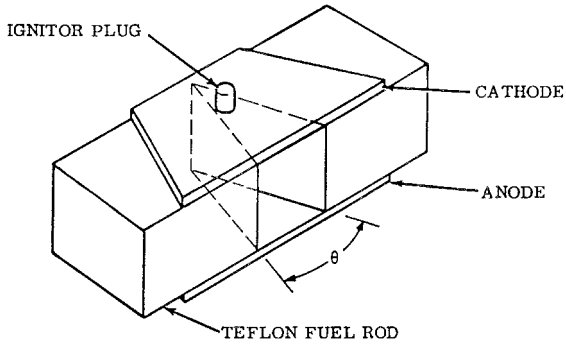

Fig. 2 Schematic of side-fed electrode-propellant configuration.

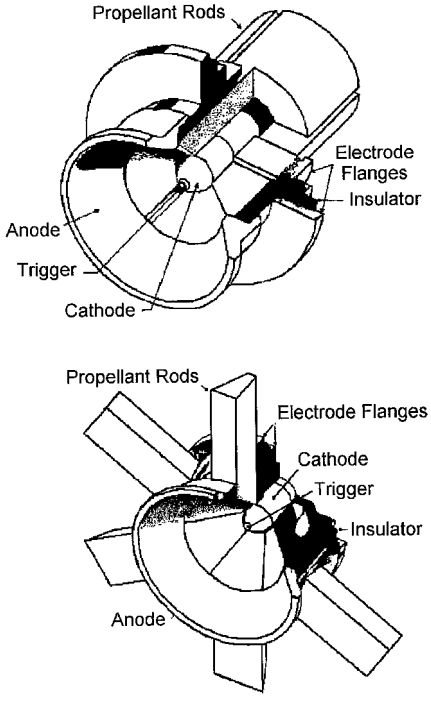

Fig. 3 Coaxial PPT geometries, originally developed for the MPD thruster.

5) Solid propellant advantages: no tankage, feedlines, seals, mechanical valves, easily measured propellant consumption, zero-*g*, cryogenic, vacuum compatible, noncorrosive, nontoxic, long shelf life, not affected by rapid temperature changes, or not affected by variable high "*g*" loads.
6) Discreet impulse bits compatible with digital logic.
7) Variable thrust level.
8) Performance compatible with attitude control and station-keeping requirements.
9) Operation at large variation in environmental temperature.
10) Thrust vector control capability.

To these we may add that the PPT is capable of providing tiny impulse bits, enabling fine attitude and position control of satellites, which is particularly important for formation flying. Furthermore, the robust design has permitted immediate thruster operation, even after many years of storage. These advantages explain why the PPT was initially employed on spacecraft, and why it continues to be developed and used today.

II. Basic Physics of the PPT

Although simple in its embodiment, the PPT unites many complex interactions resulting from electromagnetic and electrothermal processes. Pulsed operation and the three-dimensional geometry of the traditional PPT make these interactions quite difficult to assess quantitatively. Appendix A reviews basic theoretical formulations that can help in understanding PPT behavior and performance. Section XI discusses recent advances based on numerical simulations that attempt to include all processes together. The present section intends to provide a framework for subsequent discussions of PPT experiments and theory.

A. Ignition

The complexity of PPT behavior starts with the ignition of the discharge. Usually, an igniter plug provides a spark generated at a semiconducting plug surface. The energy and mass associated with this spark are much smaller than the corresponding values for the main discharge, and so the exact conditions of the igniter plasma should not directly affect the performance of the PPT. Nevertheless, conditions do matter to some degree as some shot-to-shot variation of PPT thrust may result from voltage and plug surface-induced variations in the igniter plasma. Furthermore, the position of the igniter plug relative to the surface of the propellant must necessarily be optimized empirically for each design.

To date, insufficient study has been devoted to delineating the actual mechanisms by which the igniter starts the PPT discharge. Candidate processes include simply providing an initial plasma discharge near the propellant surface. This initial discharge causes sufficient evaporation of the propellant to sustain higher currents. Alternatively, ultraviolet radiation from the igniter spark can free electrons from the propellant that initiate a discharge along its surface. Numerical simulations successfully use the former mechanism in modeling the PPT. The latter mechanism participates in the flashover of insulators subject to much higher electric fields in vacuum: typical fields are 10–100 kV/cm vs ~1 kV/cm in PPTs.

B. Main Discharge

Once initiated, the PPT discharge rapidly becomes an arc, with the voltage between the electrodes dropping rapidly to a few hundred volts. Early in the current pulse, the discharge displays filaments and spot attachment at electrodes, typical of low-current, low-pressure arcs. As the current rises to kiloamperes per cm of width however, conditions for a diffuse arc can exist. That is, there is sufficient heat transport at the low particle densities afforded by the downstream vacuum to overcome the tendency for current concentrations in regions of higher plasma temperature. Ideally, the diffuse arc covers the entire exposed surface of the propellant, providing uniform

conditions for heat transfer to, and ablation of, the propellant bar. Experiments indicate that some concavity develops on initially flat Teflon propellant surfaces, suggesting that heat transport from the arc concentrates in the middle of the surface. Tests with alternating layers of Teflon and polyethylene sandwiched between the electrodes similarly indicate nonuniform ablation along the propellant face. The relationship of the width of the discharge to the width of the exposed propellant surface remains a subject for further study and clearly can affect attempts to scale the PPT to lower or higher power levels.

The PPT plasma is composed of electrons and heavy-particles of various charge states in a condition of electrical quasi-neutrality, this is typical of an arc discharge. The electron temperature depends on a balance of resistive heating and collisional energy loss, primarily to internal states of the heavy particles and radiation. Nonequilibrium conditions exist in varying degrees and kinds because the downstream vacuum permits low particle densities and high flow speeds. In the immediate vicinity of the propellant surface, where speeds are low and densities are high, more opportunity for local thermodynamic equilibrium (LTE) exists, although the electron temperature may still differ significantly from the heavy-particle temperature (two-temperature LTE).

Further downstream, however, plasma conditions may severely test available tools for modeling flow behavior in detail. The possibility for nonequilibrium can extend to the electron velocity distribution, with microinstabilities providing high-energy electrons and higher degrees of ionization than expected based on "temperatures" associated with particle transport. Interpretations of spectroscopic measurements of the PPT exhaust plasma suffer from the complexities of these nonuniform, nonequilibrium conditions.

C. Plasma Dynamics

As an arc discharge, the PPT plasma has sufficiently high temperatures to provide interesting values of specific impulse when compared with chemical thrusters. Inelastic processes and radiation, however, limit the electron temperature to a few eV (1 eV = 11,600 K). This, in turn, limits the energy that heavy particles can attain by heat transfer from the electrons and, therefore, the value of exhaust speed associated with electrothermal operation. For example, using a stagnation temperature of 2 eV and a specific heat ratio of 5/3 for a frozen, dissociated flow of Teflon, the limiting exhaust speeds of heavy particles should not exceed about 8 km/s for carbon and 7 km/s for fluorine. Measured exhaust speeds in PPTs are much higher (>15 km/s). Thus, heating of heavy particles by plasma electrons cannot provide more than about 25% of the kinetic energy of the heavy particles. Loss of mass from the propellant surface without the opportunity for electromagnetic acceleration, e.g., after the discharge pulse or as macroparticles, can provide additional small contributions to the impulse bit of the PPT. The existence of high- and low-speed components of mass loss is confirmed by both experimental measurements and theoretical analyses of PPTs, and represents a critical characteristic in understanding PPT performance (see Secs. X and XI).

Electromagnetic forces provide the high specific impulse component of the PPT. Figure 4 displays the current flow and magnetic field pattern for a PPT in an idealized representation of its rectangular configuration. Currents in the plasma discharge and the return or "backstrap" conductor repel, causing electromagnetic acceleration of the plasma and a reaction force on the return conductor. At the same time, the magnetic field lines encircling the plasma tend to squeeze the plasma into a narrow column. The resulting forces on the plasma are described in terms of both electromagnetic field theory and circuit theory formulations in Appendix A.

Resistive heating in the discharge sustains the plasma at a high temperature, supplying energy to the solid propellant by

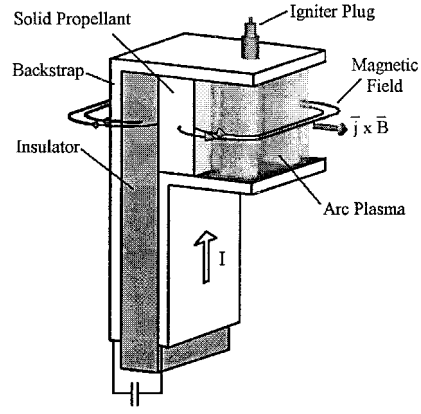

Fig. 4 Idealized representation of a rectangular PPT configuration, showing plasma current and magnetic field lines.

heat conduction and radiation. Energy deposition in the solid propellant liberates material, an unknown fraction of which participates in the plasma discharge. Heat transfer to the thruster and spacecraft structure (and to space by radiation) accounts for energy not used by mass ablation. Note that the transfer of energy from the discharge to the solid propellant generally depends on the relative position of the discharge. Thus, understanding PPT behavior and performance requires a self-consistent solution of equations for plasma dynamics, transport, and electrical circuitry.

Two limiting modes of discharge operation can occur, depending on the details of the heat transfer and acceleration process. For sufficient heat transfer, the propellant surface provides new electrically conducting material, so that the discharge path can remain adjacent to the propellant surface in a stationary "ablation-arc" mode.[22] Otherwise, the discharge must follow the accelerated material at high velocity, so that the PPT operates in the "propagating" or "slug" mode. The alternative term "deflagration" is sometimes used for the former mode. For discharges driven into a gas, the term "detonation" might apply to the latter mode, except that the PPT plasma propagates into vacuum. A combination of modes may also occur in which the propagating plasma discharge causes sufficient voltage near the propellant surface to allow a second discharge (a "restrike") that remains stationary in an ablation-arc mode.

Traditionally, the PPT operates with an oscillatory current waveform, closely resembling that of an LRC circuit. Coupling of magnetic flux to the plasma flow, therefore, can result in higher magnetic fields in the plasma than provided by the instantaneous current in the external circuit. The plasma effectively experiences acceleration by a magnetic piston that oscillates (with decreasing amplitude) as currents in the upstream portions of the flow are alternately repelled and attracted by currents in the backstrap conductor. From a field point of view, the magnetic pressure gradients in the plasma can reverse direction when the circuit current decreases. Such oscillating acceleration adversely affects the performance of the PPT, if ablated material does not achieve a uniformly high speed. The opportunity for plasma currents to differ from the current in the external circuit also interferes with attempts to model PPT performance using circuit equations and simple plasma dynamics, e.g., slug model. Magnetohydrodynamic (MHD) calculations, of course, can follow current and field variations self-consistently.

D. Mass Loss

The PPT can lose mass in several ways and on several time scales. These include simple evaporation during and following the discharge pulse, the expulsion of macroparticles, and erosion of electrodes and the igniter plug. The various masses can have quite different velocities. Consideration of PPT perfor-

mance and its improvement must attempt to delineate such differences from past and future data that usually only provide total mass loss and thrust impulse over many firings.

Exposure of the propellant surface to the arc discharge increases the propellant temperature near the surface, leading to higher rates of evaporation toward the downstream vacuum. The equilibrium vapor pressure scales in an exponential fashion with temperature

$$p_{eq} = p_c \exp(-T_c/T_s) \tag{1}$$

where p_c and T_c are characteristic pressure and temperature values, respectively, for the material; and T_s is the surface temperature. For Teflon, $p_c = 1.84 \times 10^{15}$ N/m^2 and $T_c = 20{,}815$ K.[23,24] The high value of T_c for Teflon indicates that modest changes in surface temperature can result in very large changes in evaporation rate. This suggests that the details of heat transport to the surface from the arc critically affect the time scale for providing mass to the discharge. Different behavior, therefore, might result from small changes in the operating and design parameters of the various PPTs. Curiously, however, some general consistency exists in terms of mass loss per joule of stored energy over broad ranges of conditions. This uniformity allows speculation[24] that the mass production is determined by constraints of the overall flowfield, e.g., sonic conditions, instead of depending closely on fine-scale structures, e.g., temperature-gradient scales.

Such speculation obtains further credence from recognition that the amount of energy needed to evaporate propellant represents only a very small fraction of the energy needed to dissociate, ionize, and accelerate the resulting vapor. The heat of vaporization for a polymer[25] comprises the phase transition h_f to a gas, the depolymerization or "unzipping" of the polymer chain h_d, and the heating of the gas to arc temperature

$$h_v = h_f + h_d + c_p \Delta T \tag{2}$$

For Teflon, h_v equals about 2×10^6 J/kg, with three-quarters because of $h_f + h_d$. An exhaust speed of 15 km/s corresponds to a kinetic energy per unit mass of about 10^8 J/kg. Thus, evaporation requires only about 2–4% of the energy needed to accelerate propellant to speeds characteristic of specific impulse values (1000–1500) for the PPT.

Not all the material leaving the surface, however, attains the high speeds that provide such specific impulse. Increasing the surface temperature, to supply even a small amount of mass for electromagnetic acceleration during the discharge pulse, demands the deposition of heat within the propellant. Simple heat conduction relates the total heat delivered in the propellant to the product of surface temperature and thermal-diffusion depth. (Radiative transport may modify the details, but the temperature distribution still peaks at the surface.) The surface, therefore, will continue to evaporate long after completion of the discharge pulse, providing mass that cannot experience acceleration to high speeds by electromagnetic and gasdynamic forces. The fraction of mass participating in this late-time ablation is not well understood. Furthermore, high temperatures at the surface during the discharge pulse imply the opportunity for sufficiently high temperatures below the surface for decomposition or phase-change of the propellant. Such changes in the presence of a pressure pulse from the PPT can result in additional loss of material at low speed in the form of droplets or other macroparticles. Experiments by Spanjers et al.[26] suggest that perhaps 40% of the mass loss from the PPT is in the form of low-speed macroparticles that do not contribute significantly to the impulse bit.

The thruster electrodes and sidewall insulators also provide material to the PPT flow. Some of this material participates in the overall electromagnetic acceleration of plasma during the discharge pulse. Other mass, however, may evolve later as surfaces cool (or erupt) following the heat pulse and particle bombardment from the discharge.

Review of the large number and variety of PPT experiments, and their interpretations, requires considerable care because of the several possible velocity components and time scales associated with mass evolution. By identifying aspects of PPT operation that presently limit performance, we can then look forward to directions for improvements.

III. PPT Types

PPTs may be classified in a 2 × 2 matrix of four types:

Rectangular	Coaxial
Breech-fed	Side-fed

A common configuration is the breech-fed PPT with parallel rectangular electrodes, driven by a long current pulse, as typified by the LES-8/9 and EO-1 thrusters. For the rectangular electrode configuration, the current and self-induced magnetic field are primarily transverse to the flow. The anode and cathode arc attachment regions are then free to move downstream along the electrodes with the flow.

The coaxial configuration is usually conical, typically with central and downstream ring electrodes. In any PPT the igniter plug is usually mounted in the cathode (we have found no exceptions to this rule), which in the coaxial version can be either the center electrode or the downstream ring. Coaxial arrangements of ablation-fed, plasma thrusters (Fig. 3) were originally developed as MPD devices.[19] The outer ring electrode is usually narrow, so that the current anchors at a definite location. Modest values of magnetic Reynolds number result in a limited downstream extension of the current pattern.

The discharge resistivity is determined by the electron temperature, and the discharge resistance depends on the resistivity and the geometry. In the limit of magnetic Reynolds number based on an electrode length much larger than unity, the streamwise extent, i.e., thickness, of the discharge is determined by the flow speed divided by the resistivity. The resistance is then proportional to the back electromotive force ($-\boldsymbol{u} \times \boldsymbol{B}$) divided by the current. By varying the electrode diameter, azimuthal symmetry in the coaxial PPT gives better control over resistance than does the rectangular geometry, for which the current density is not as well known.

Whether the PPT is breech-fed, as early versions were, or side-fed, developed later (Fig. 2), influences whether the PPT operates in the ablation arc or propagating mode. These two operating modes closely resemble deflagration and propagating modes in electromagnetic pulsed plasma devices either using gas injection, such as the coaxial "Marshall" gun,[27] the parallel plate configuration,[28] the high repetition rate PPT,[29] the coaxial plasma accelerator,[30] and the pinch engine,[31] or using prefills such as the linear pinch.[32] The gas-fed plasma accelerators inject mass in the upstream region, which has the effect of supplying current carriers at the breech of the device. The injected mass is then ionized by a combination of radiation and electron collision.[33,34] Devices of this type also include the MPD thruster and the deflagration gun.[35,36] With sufficient current carriers supplied upstream, the current distribution can become stationary, similar to the deflagration mode of combustion observed with flames.

The breech-fed PPT, such as the LES-6, features a current distribution that initially propagates downstream at a speed greater than the mass-average velocity, suggesting that the mass rate of ablation at the rear of the arc is not sufficient to provide spatial stabilization. In the breech-fed PPT the primary $\boldsymbol{j} \times \boldsymbol{B}$ force vector points away from the ablating surface, so that when the arc strikes it moves off the surface, reducing the ablation rate. On the other hand, for side-fed devices, the $\boldsymbol{j} \times \boldsymbol{B}$ vector is parallel to the ablating surface, and the B field lines are normal to it, providing a conduit for electrons to reach the Teflon and maintain the ablation rate. Thus, a downstream mo-

Table 1 Thrust and mass ablation characteristics of various PPTs

Thruster	E_o, J	Type	I_{sp}, s	I_{bit}, μN-s	I_{bit}/J, μN-s/J	$\Delta m/E_o$, μg/J	Δm/area, μg/cm^2
LES-6	1.85	Breech-fed	300	26	14	4.8	3.3
SMS	8.4	Breech-fed	450	133	15	3.4	3.9
LES-8/9	20	Breech-fed	1000	297	15	1.5	4.8
TIP-II(NOVA)	20	Breech-fed	850	375	19	2.3	5.7
MIT Lab	20	Side-fed	600	454	23	2.8	4.3
MIPD-3	100	Side-fed	1130	2250	23	2.0	4.3
Millipound	750	Side-fed	1210	22,300	30	2.5	27.7
Primex-NASA	43	Breech-fed	1136	737	17	1.5	2.6
IL PPT-3 Lab	7.5	Coax-side-fed	600	450	60	10.0	36.0
Japan Lab	30.4	Breech-fed	423	469	15	3.7	6.4
China Lab	23.9	Breech-fed	990	448	19	1.9	5.3

tion of the side-fed PPT, to first order, does not change the ablation rate.

In addition to the four basic geometric and propellant feed variations, PPTs are also distinguished by variations that include short pulse vs quasisteady; ablation area; the location and type of the igniter plug; alternate propellants other than Teflon; parallel vs flared rectangular electrodes; ablating, nonablating, and conductive nozzles; oscillatory vs nonoscillatory current; and applied magnetic field. These distinctions create different operating modes for the PPT, affecting the impulse bit and specific impulse, and all must be considered in a PPT design. A brief discussion of each is given here.

Short pulse vs quasisteady: In most PPTs the pulse length is generally long, in that the pulse length t_p is greater than the streamwise acoustic time L/a in the thruster, allowing the pressure to follow the instantaneous power input. Typically L is 2 cm and a is 5000 m/s, giving $L/a = 4$ μs, compared with $t_p = 20$ μs. In the limit $t_p >> L/a$, the flowfield properties vary in quasisteady fashion along with the thruster current. The time scale for ejection of the thermal plasma from the thruster is therefore governed more by the pulse length than the sonic velocity. In the short pulse limit $t_p << L/a$, the electromagnetic component of thrust is applied in time t_p, followed by the gasdynamic component on a time scale L/a.

Ablation area: PPTs can be rated by the specific mass ablation (ablated mass per joule), with a lower value of this parameter generally associated with higher specific impulse. This quantity is shown in Table 1 in units of μg/J. The table also displays the μg of ablated propellant per exposed area of Teflon for various PPT types.

Igniter plug: The breakdown is initiated with a plug, usually of the semiconductor type, located in the cathode. The plug discharge energy is a fraction of a joule, and is supplied by a silicon-controlled rectifier-switched ~1-kV capacitor circuit. The plug is usually coaxial, and the breakdown is a spoke at an azimuthal location that varies from shot-to-shot, which, in turn, can produce shot-to-shot variations in the main discharge pulse.

Propellant: After testing of several dozen alternatives, the propellant producing the best performance in a PPT is Teflon. Teflon provides attributes of high I_{sp}, high impulse bit, and zero surface char. The search continues for alternatives with better characteristics; see Sec. VII.

Parallel vs flared electrodes: In the rectangular geometry the plane electrodes are usually parallel, but for some thrusters the performance is improved by angling the electrodes away from the thrust axis, providing a nozzle effect (Fig. 5). The resulting reduced plasma density may also benefit electromagnetic acceleration of the plasma.

Nozzle: Use of a high area-ratio nozzle-electrode combination in a coaxial PPT can increase both electromagnetic and gasdynamic thrust components. Coaxial versions of the PPT exist in several versions, all employing a high area ratio nozzle, usually conical. The nozzle can be metallic, in which case it is attached to or comprises the cathode. A number of coaxial

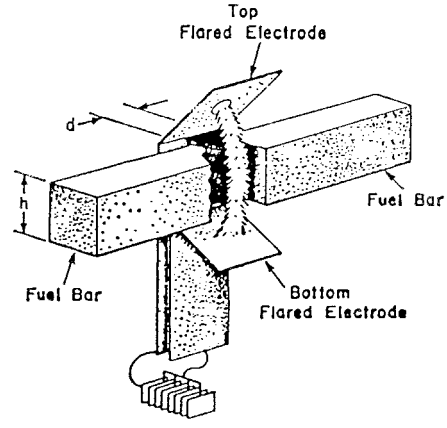

Fig. 5 Side-feed thruster with flared electrodes.

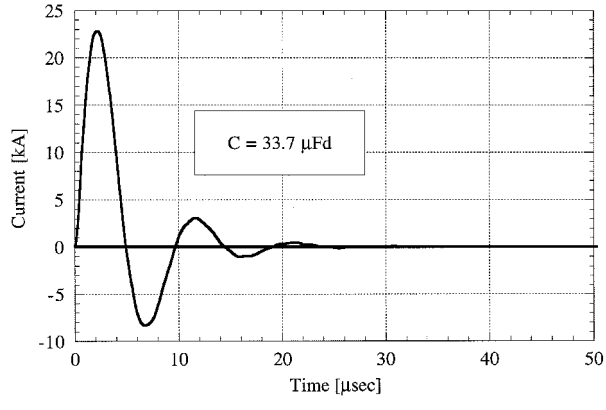

Fig. 6 Typical PPT current pulse. The oscillations reduce thrust and capacitor life.

devices use a Teflon nozzle, which then continuously ablates, and which may or may not achieve an equilibrium contour. A third version uses a nonablating ceramic nozzle, with the Teflon propellant introduced upstream of the throat. With a Teflon or ceramic nozzle the cathode is a thin annular ring at the nozzle exit plane.

Pulse shape: Because the external (LRC) circuit impedance can exceed the discharge impedance, the PPT current pulse generally oscillates in the manner of a damped sine wave, achieving 2–4 half-cycles before the remaining voltage is insufficient to break down the electrode gap (Fig. 6). This mode, sometimes called bipolar, can produce regions of reverse $\boldsymbol{j} \times \boldsymbol{B}$ in the plasma, and the oscillating voltage forces a tradeoff between lifetime and capacitor mass. Current reversal also increases electrode sheath losses and heat transfer. A better pulse shape is the nonreversing unipolar pulse, which is achieved through one of several techniques employing a passive (pulse forming) or actively switched external circuit (see Sec. XII).

For coaxial geometries the PPT impedance can be high enough to reduce or eliminate current oscillation.

Applied magnetic field: For rectangular PPTs, an applied field parallel to the field that is self-induced by the current will enhance the $\boldsymbol{j} \times \boldsymbol{B}$ acceleration. The field can be supplied by electro- or permanent magnets.

IV. Early Experimental History

The earliest known pulsed thruster came from Russia in 1934.[37] This thruster developed gas pressure by discharging capacitively stored energy into a plenum lined with plastic, using a converging–diverging metallic nozzle to expand and accelerate the resulting gases. It is not known if thrust measurements were obtained, but because of the configuration, the acceleration mechanism was purely electrothermal. A number of early devices were gas-fed[38] or fed with a soft wax.[39]

Antropov and Khrabrov in the USSR, beginning in 1962, developed two PPT designs, one with an electromagnetic and one with a thermal acceleration mechanism (Fig. 7). The latter version was integrated on the Zond-2 spacecraft and was launched in 1964. In the U.S., PPT development was led by the pioneering work of Guman and Palumbo, at the Fairchild Republic Company, and of Solbes, Thomassen and Vondra, at the Massachusetts Institute of Technology Lincoln Laboratory. These efforts consisted of experimental research to understand basic PPT physics, as well as development and flight qualification of PPTs. On Sept. 26, 1968 the first U.S. PPT spaceflight was achieved on the LES-6 satellite, for which the thruster performed attitude control. In the U.S., the stimulus for the LES-6 PPT with solid Teflon propellant came from early efforts (1965) to integrate onto a satellite a 360-μN thrust gas-fed PPT that failed because of the mechanical metering valve. The PPT systems in use today are similar to those employed in the Zond-2 and LES-6.

During the 1970s and 1980s, when much of space technology in the U.S. languished in a post-Apollo twilight, studies continued on the PPT and related thrusters. One example was the attempt to extend the successful low-energy PPT to the millipound range,[40] (1 mlb = 4450 μN) by operating at a higher energy per pulse, and required conquering several problems with igniter plug and electrode degradation. By the end of the millipound program, capacitor lifetime remained the principal technological hurdle, and voltage reversal and capacitor overheating appeared as the major cause for failure at lifetimes far short of the design goal. Also, during the midseventies, advanced PPT concepts achieved increased levels of performance, including[41] side-fed arrangements that achieved 41 μN-s/J at a specific impulse of 1500 s, and end-fed systems that achieved 21 μN-s/J at 5160 s. Nevertheless, at the end of the decade U.S. Air Force funding shifted to other needs, before the millipound engine and advanced PPTs developed into flight hardware. On the other side of the Pacific, the Chinese[42] performed a suborbital test of a PPT.

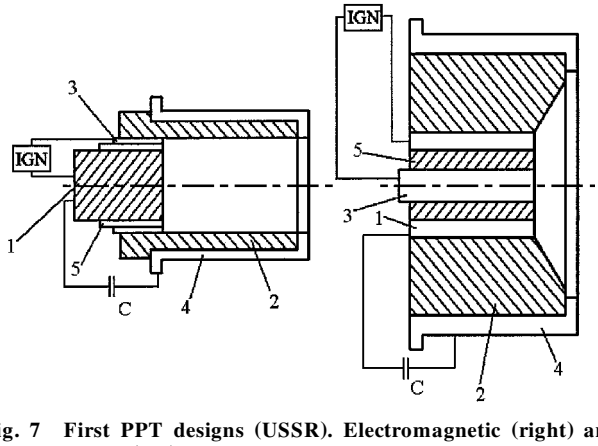

Fig. 7 First PPT designs (USSR). Electromagnetic (right) and electrothermal (left).

During this time, work continued in Italy[43,44] on ablation-fed coaxial MPD thrusters and also in Japan[45–47] and China.[48] The former activities used ablation to avoid the difficulties of developing a gas valve for repetitive operation for millions of shots. The Japanese studies, by several authors, included mass-spectroscopic analyses,[47] and extension of traditional PPT arrangements to include applied magnetic fields,[45,46] resulting in 17 μN-s/J at a specific impulse of 4000 s.

By the early 1980s, electric propulsion had failed to develop as a means of primary space propulsion, even though laboratory research and development had continued for four decades. Thus, the PPT remained the only electric thruster with a continued application as onboard propulsion for an operational vs scientific test mission. A strategy for electric-propulsion development was then proposed, using the PPT as the starting point for a family of robust, simple electric thrusters with increasingly ambitious goals.[49,50] The PPT would provide a controlled, repetitive source of plasma that would actuate later stages of electromagnetic acceleration, using passive circuitry in which the switching occurred when the plasma arrived. A two-stage PPT demonstrated the basic concept,[51] using a constant current pulse-forming network to drive an ablation-fed, rectangular thruster as the second stage. This second stage ignited after receiving plasma from a flight-qualified model from the 1960s LES-8/9 series. The design energy of the second stage could increase as needed for higher energy missions. The family of thrusters as a whole, however, would share flight experience back to the LES series, thus countering the argument that new electric propulsion systems lacked flight experience.

At the time this strategy was proposed, the possibility of steady power levels in space of upward of 100 kW still captured the attention of much of the electric propulsion community.[52] Despite warnings of another "false dawn" that would leave electric propulsion still without primary propulsion experience, the promise of steady electrical power in space overcame the actuality of success with smaller pulsed electrical systems. With the (temporary) demise of space-based nuclear power, and the increase in missions with modest, solar electrical power levels, interest has rekindled in the PPT.[53,54]

The measured performance of a number of PPTs is given in Table 1, with pulse energy ranging from 1.85 to 750 J, for breech-fed and side-fed thrusters. The thrust, measured in terms of impulse bit per joule, is plotted vs I_{sp} in Fig. 8. With the exception of the PPT-3, which will be discussed separately, the thrusters mainly fall either into a high I_{sp} group at 1100 ± 100 s at 15–30 μN-s/J, or a lower I_{sp} group at 450 ± 150 s at 14–23 μN-s/J. Two thrusters operating at $I_{sp} > 4000$ s are also reported (Fig. 8). Most thrusters (Table 1) ablate in the range 1.4–5.3 μg/J, and the mass ablated is 4.5 ± 1.9 μg/cm^2, suggesting relatively similar ablation mechanisms for all types. These data basically derive from measurements of steady thrust during repetitive firing of the PPT and subsequent measurements of mass lost by the propellant slab. Appendix B

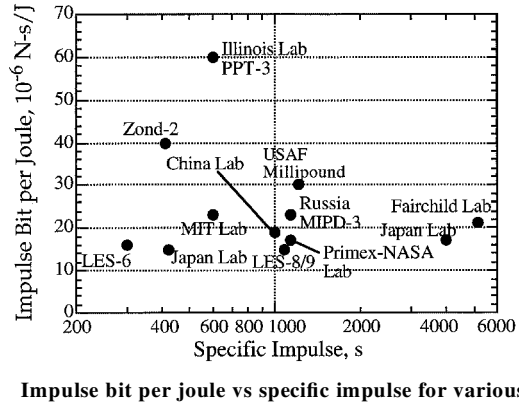

Fig. 8 Impulse bit per joule vs specific impulse for various flight and laboratory PPTs.

discusses the design and operation of thrust stands for PPT evaluation. The subject of mass loss directs attention to the thermal environment of the PPT, which depends on the repetition rate and energy per shot. The data summarized in Table 1 do not account for variations because of repetition rate.

V. Flight Thrusters

A. Zond-2

The first flight PPT, used for attitude control on the 1964 Zond-2 mission, was a breech-fed, coaxial "erosion type" design, with six thrusters on the spacecraft. The PPT used twin bars of 70-mm-long cylindrical Teflon tubes (0.4 kg), each of which was contained in a 60-mm-i.d. thin-wall tube of aluminum alloy that formed the anode. Total system mass was 5 kg. The central cathode was a 20-mm-diam copper rod. The thrust mechanism was primarily electrothermal, and the space qualification test was 10^6 pulses. Performance parameters are given next. Parameters of PPT for Zond-2: stored energy = 50 J, capacitor voltage = 1.0 kV, igniter system voltage = 1.0 kV, PPU efficiency = 0.8, pulse rate = 1.0 Hz, specific impulse = 410 s, thrust at 1.0 Hz = 2 mN, and impulse bit/J = 40 μN-s/J.

B. LES-6

The LES-6 PPT was launched in 1968, and achieved 10 years of operation in orbit. In the early development of PPTs it was recognized that gasdynamic pressure played an important role in producing thrust. Measurement of the magnitude of the gasdynamic contribution on the LES-6 thruster was provided by Solbes and Vondra,[55] who measured thrust impulse and mass consumption while experimentally varying parameters of the external circuit: electrode gap d = 3.0 cm, width b = 1.0 cm, length 0.6 cm; capacitance from 0.66 to 6.0 μF; voltage from 500 to 2000 V; external resistance from 0 to 0.80 Ω; external inductance from 50 to 650 nH. Under these conditions the ablated mass varied from 1 to 17 μg/pulse. It was then proposed[55] that the impulse bit be represented in the form (adopting $dL/dx = L'$):

$$I_{\text{bit}} = \Delta m U_0^* + \frac{1}{2} L' \int I^2 \, dt \tag{3}$$

where the velocity and the inductance gradient are determined by a curve fit to the data. The results were U_0^* = 1225 m/s and L' = 0.253 $\mu_0(h/d)$ = 0.95 μH/m.

The impulse bit and ablated mass of the LES-6 at 540 s are shown vs energy in Fig. 9. Depending on the circuit parameters, the measured specific impulse was in the range of 200–590 s, of which 125 s was the gasdynamic contribution. At 500 s the electromagnetic contribution was 375 s, and the gasdynamic contribution was therefore 25%.

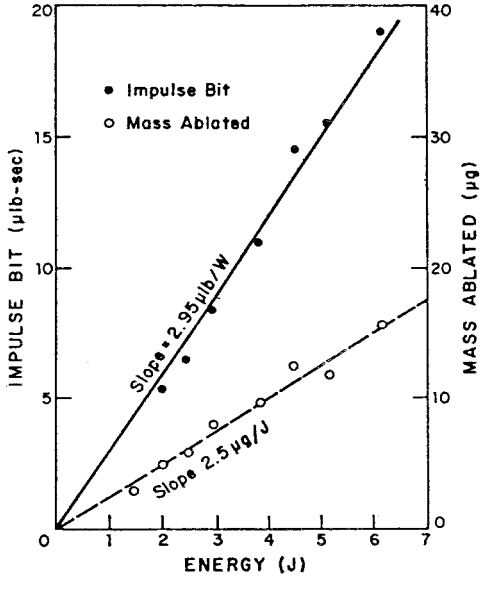

Fig. 9 Impulse bit and ablated mass of the LES-6 vs energy.

C. SMS

The PPT designed for the SMS provided more thrust than was available from LES-6. This PPT had variable thrust capability and was used for spin axis precession control.

D. LES-8/9

The LES-8/9 PPT was flight qualified for launch in 1975, but ultimately was not on the mission.[6] All propulsion on the 454-kg satellites was to be delivered by six PPTs, which were to provide attitude control, stationkeeping, and station changing. Parameters of the LES-8/9 PPT are provided in Table 2.

In laboratory tests the impulse bit was found to vary from 267 to 352 μN-s, averaging 297 μN-s over 2 × 10^7 pulses. This variation was caused by intentionally varying the location of the spark in the annular plug gap, from 2 to 11 mm from the propellant face, causing a correspondingly large variation in ablated mass from 36 to 26 μg/pulse.[6] Impulse bit varied only slightly with spark position, from 325 μN-s at 2 mm to 316 μN-s at 7 mm, but specific impulse rose sharply from 925 s at 2 mm to a maximum of 1150 s at 7 mm, falling for larger distances. Shot-to-shot variation in the impulse bit was improved by a plug design that stabilized the spark location.

The LES-8/9 was also tested at four times the energy (80 J, 3000 V) and one-fourth the pulse rate (0.25 pps), keeping power constant. The specific impulse was 1450 s, an increase of 35%, and the impulse bit increased a factor of 5.1 to 1500 μN-s indicating an increase in efficiency. Capacitor life at the higher voltage diminished to 10^7 pulses, vs 10^{11} pulses at 1500 V.

E. TIP-II (NOVA)

Two TIP-II PPTs were used to provide drag compensation on the NOVA series of satellites, which flows in a phased constellation within a 2-mm deadband in a 640-n mile orbit.

Table 2 Specifications of the LES-8/9 PPT

Type	Rectangular, parallel plate, breech fed, twin fuel bars	Total firing rate	1 or 2 pps
Thrust axis	Canted 30-deg to thruster axis	Specific impulse	1000 s
Fuel	Rectangular Teflon bars	Igniter plug	Coaxial semiconductor
Stored Energy	20 J	Igniter voltage	625 V
Capacitor	Mylar–paper–oil, 17 μF at 1538 V	Igniter energy	0.4 J
Power Conditioner	20-kHz flyback	Mass/pulse	30.3 μg/pulse
PPU efficiency	80%	Thruster total mass	6.60 kg
Bus power at 1 pps	25.5 W	Electronics mass	0.91 kg
Peak current	18,000 A	Fuel mass	0.75 kg
Total impulse	7320 N-s	Capacitor mass	1.93 kg
Impulse bit	297 μN-s	Structure mass	3.01 kg

Performance of this 20-J system, with 0.45 kg of Teflon per thruster, is given in Table 1.

VI. Selected Laboratory Thrusters

A. Russian MIPD-3 PPT

The work of Antropov et al.[56,57] includes performance measurements on the MIPD-3 thruster, plus detailed diagnostics of the arc and plume. The thruster is a side-fed device with an I_{sp} of 1130 s and impulse bit of 2250 μN-s at 100 J. During the first half-cycle, magnetic probes showed no current density at the back insulator, and a $\boldsymbol{j} \times \boldsymbol{B}$ current front moving in the flow direction at 20–25 km/s, from which it was concluded that the B-field lines were frozen into the plasma. A completely different behavior was displayed during the second half-cycle, for which the current distribution was stationary, with a maximum along the back insulator. This suggests that the arc was operating in a propagating mode for the first half-cycle and a deflagration mode for the second.

The magnetic and gasdynamic pressures were estimated from current, density, and pressure data. The maximum magnetic pressure was on the order of 10 atm, and the gasdynamic pressure on the order of 0.2 atm, suggesting that the thrust mechanism of the MIPD-3 is predominately electromagnetic.

B. Japan

Kimura et al.[45,48] demonstrated control over the relative electromagnetic and electrothermal contribution in a rectangular PPT by applying a magnetic field parallel to the self-induced field, to increase or decrease the field strength. Both electromagnets and permanent magnets were used, up to 0.57 T. An applied magnetic field of opposite polarity reduced the $\boldsymbol{j} \times \boldsymbol{B}$ force, increasing mass/pulse and impulse bit, the latter by as much as 66%. It was concluded that this retarding field increased the electrothermal contribution because the impulse bit increased with reduced $\boldsymbol{j} \times \boldsymbol{B}$.

C. China

In China, An et al.[42] designed, built, flight-qualified, and launched the MDT-2A PPT on a sounding rocket, the first Chinese launch of a pulsed plasma thruster. Yuan-Zhu,[48] working with a parallel plate, breech-fed design, performed parameter studies to show the effect of electrode geometry and energy on performance. A sample of the data is shown in Table 1. The electrode spacing-to-width ratio h/w was shown to affect performance significantly. For 23.9 J, increasing h/w from 1.38 to 4.50 increased I_{bit} by 47% to 448 μN-s, and I_{sp} by 35% to 990 s. This result is consistent with the increase in L' by 65% for this variation in h/w.

D. Fairchild

Guman,[25] working with a breech-fed PPT, developed an analytic formulation that treated the impulse bit as the sum of electromagnetic and electrothermal contributions:

$$I_{bit} = \frac{1}{2} L' \int i^2 \, dt + \left[\frac{8(\gamma - 1)}{\gamma^2(\gamma + 1)} \Delta m E_o \right]^{1/2}$$

where, for Teflon ($\gamma = 1.3$), the γ function = 0.79. This expression is only approximate because it assumes that the flow expansion occurs at constant area, and that all of the energy E_o is added to the arc before any mass Δm ablates, a condition that does not hold unless the discharge pulse length is on the order of 1 μs. This model led directly to the prediction[25] that the impulse bit will be improved by the addition of a nozzle.

Using the same PPT, early work on igniter circuits began with the Krytron tube, but was dropped because of limited Krytron life (1.3×10^7 discharges) and its 4-kV voltage requirement, in favor of a 3-kV sealed spark-gap system, which exceeded 1×10^8 pulses in life tests.[25] Although the sealed spark-gap system is still in use today for turbine ignition on modern jet aircraft, the favored system now uses a silicon-controlled rectifier for switching, coupled to a semiconductor-type plug, enabling voltages of 1 kV or less. Life-cycle tests were performed on this type of system for 1.5×10^8 pulses on the igniter circuit and 7×10^6 discharges on the 17-J/kg capacitors, with 2160 N-s of impulse delivered over 3800 h on a single set of electrodes.

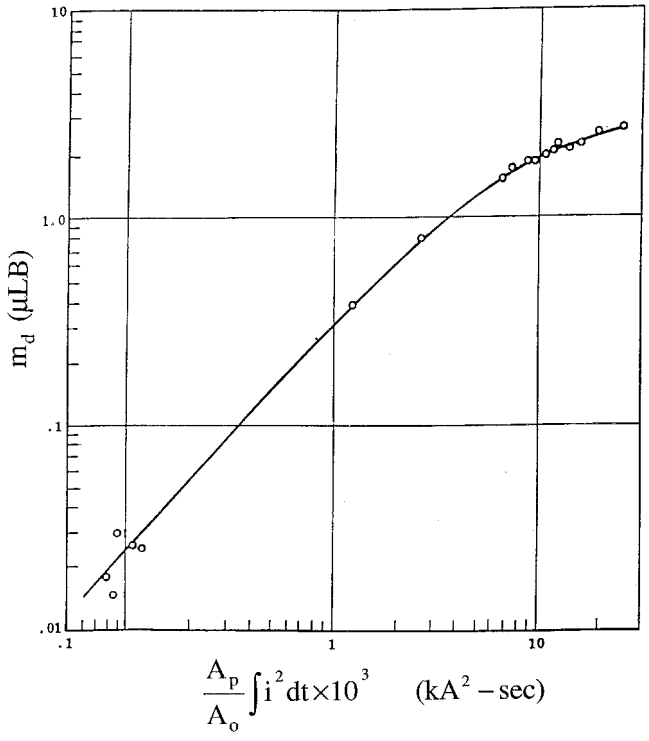

Fig. 10 Ablated mass per discharge as a function of $(A_p/A_o) \int i^2 \, dt$.

E. Side-Fed

Vondra and Thomassen[18] tested a 20-J side-fed PPT by varying the spacing between the two propellant bars, resulting in a variation in the mass per pulse. For 9 μg/pulse, the impulse bit was 227 μN-s at 2580 s, and for 56 μg/pulse, the impulse bit was 454 μN-s at 600 s. It was concluded that the doubling in impulse bit at 20 J was because of the gasdynamic pressure thrust, which is approximately equal to the $\boldsymbol{j} \times \boldsymbol{B}$ thrust at 600-s specific impulse.

In further side-fed PPT work at the 300-J level, Palumbo and Guman[59] evaluated geometries for which the facing propellant bars were angled to form a "V" shaped cavity (Fig. 2). A typical I_{sp} was 700 s. For included V angles between 0 deg (parallel walls) and 80 deg, the thrust/power ratio was highest for 0 deg, and was 11% higher at 0 deg than at 40 deg. In a propellant ablation study, it was demonstrated that the ablated mass correlated with the parameter, $(A_p/A_o) \int_0^\infty i^2 \, dt$, where A_p is the ablating area of the propellant exposed to discharge radiation, and A_o is the open area at the plasma boundaries through which radiation escapes (Fig. 10). The correlation holds over a range of two orders of magnitude in the parameter, for ablated masses from 7 to 600 μg/pulse. The quantity $\int_0^\infty dt$ is observed to equal the stored energy divided by circuit resistance for a fixed LRC circuit

$$\int_0^\infty i^2 \, dt = \frac{E_o}{R} \tag{4}$$

Although the total resistance R is not known a priori, it was found that the current integral could be represented as

$$\int_0^\infty i^2 \, dt = 1.3 E_o \Big/ \sqrt{\frac{L_o}{C}} \tag{5}$$

Table 3 Semiempirical PPT design equations

Configuration	I_{sp}, s	$I \times I_{sp}$, μN-s^2
Breech-fed	320 $(E_0/A_p)^{0.6}$	2500E$^{1.6}$
V-shaped	320 $(E_0/A_p)^{0.6}$	1660E$^{1.6}$
Side-fed	320 $(E_0/A_p)^{0.6}$	1120E$^{1.6}$

where $\sqrt{L_0/C}$ is called the initial impedance, and L_0 is found at $t = 0$ from $L_0(di/dt) = V_0$, typically in the range of 100–200 nH.

Semiempirical equations for a particular PPT design were provided by Guman,[60] based on the experimental results for breech-fed, V-shaped, and side-fed configurations (Table 3). Correlations were found both for the specific impulse and for the product of I_{sp} and impulse bit in terms of the stored energy E_0 (J) and the exposed propellant area A_p (cm^2). The principal result is that the I_{sp} is independent of the geometry. The product of impulse bit and I_{sp} is geometry dependent, with less thrust being developed for side-fed than breech-fed devices.

F. One Millipound Thruster

Performance studies were made by Palumbo and Guman[41] on a high-energy (450–750 J) rectangular PPT driven by a 108-μFd pulse-forming network with external circuit parameters of R_{ext} =2.6 mΩ and L_{ext} = 60 nH. Both breech and side-fed modes were examined, and interelectrode spacing and electrode included-angle were varied, all at 450 J. For all of the side-fed tests, the transverse spacing between the rectangular propellant bars was held constant at 9.3 mm, the axial propellant length was 31 mm, and the electrode spacing was 76 mm. Ablated mass was found to increase monotonically with a parameter correlating the exposed propellant area and $\int i^2\,dt$. A maximum impulse bit of 16.7 mN-s (37 μN-s/J) was found at a 20-deg included electrode angle, at 1210-s specific impulse, with an ablated mass of 1.4 mg/pulse. Operating in the breech-fed mode at the same energy reduced the ablated mass 90% and raised the specific impulse over 5000 s, at about half the impulse bit.

The impulse bit[41] was separated into an electrothermal and an electromagnetic component, but the inductance gradient L' was considerably overestimated. At a reasonable L' = 0.7 μH/m and a typical current integral of 20,000 A^2-s, I_{EM} is 14 mN-s, accounting for nearly all of the impulse bit. The electrothermal component of the impulse bit, predicted as $\sim 0.8(2\Delta m E_{ET})^{1/2}$, accounts for the remaining impulse bit if Δm = 80% of the total ablated mass (side-fed mode) and $E_{ET} \cong 5$ J. The low energy may indicate a large heat loss to the walls in this thruster.

In a related effort,[61] the impulse bit was analyzed in terms of the gasdynamic and electromagnetic contributions. The impulse bit was found to vary linearly with λ, where

$$\lambda = \frac{\mu_0 \int i^2\,dt}{\sqrt{8 m_d E_0}} \tag{6}$$

is proportional to the ratio of electromagnetic to gasdynamic impulse bit, and m_d is the mass ablated per pulse. The energy required to ablate Teflon was given as 4070 J/gm, and is typically a few percent of the discharge energy.

A PPT called the Millipound Thruster,[40] developed for the U.S. Air Force, was a 750 J, side-fed PPT. The impulse bit was 22,300 μN-s. System development called for 14 × 10^6 pulses, but <10^5 discharges were achieved at capacitor failure, possibly because of a negative current reversal of 30 kA experienced in the external circuit. With the higher energy of operation over the anticipated mission, propellant handling needed to advance beyond relatively short, straight bars of Teflon, leading to the use of spiral propellant bars.

Performance data are reported by Arrington et al.[62] for a Primex Aerospace Co. breadboard PPT with flat or V-shaped propellant and parallel or flared electrodes, for which the impulse bit is generally 17 μN-s/J up to 54 J. Best performance in terms of thrust-to-power ratio was achieved with a notched fuel face in the Teflon propellant, but this approach introduced difficulties with the fuel feed system design.

G. Coaxial PPTs

Separate lines of study and experiment have proceeded for many years in which ablation of solid propellant provides a convenient way to avoid gas valves for pulsed or quasisteady plasma devices, using coaxial geometry. Work is ongoing at the University of Rome on a coaxial MPD Thruster,[44] and a group at the Russian Research Center, Kurchatov Institute, Moscow, uses coaxial PPTs for studies of plasma processing of materials.[63]

Earlier work on the pulsed electrothermal thruster (PET)[64] and the pulsed arcjet[65] now extends to an arrangement in which two, side-fed Teflon bars form the boundary of a discharge channel, providing mass flow to a coaxial PPT accelerator. Its present embodiment uses a solid-state diode in parallel with the energy-storage capacitor (Fig. 11).[66,67] Early versions of this thruster (Fig. 12) are distinguished by high impulse bit per joule (Fig. 8) and an acceleration process dominated by gasdynamic thrust.

Operation of quasisteady MPD thrusters with mass flow provided by azimuthally discrete bars of ablating solid-propellant (Fig. 3) demonstrates that the propellant feed system need not demand a rectangular electrode geometry.[19,44] While issues certainly will remain regarding the development of azimuthal symmetry within the thrust chamber, these do not differ greatly from equivalent concerns in gas-fed MPD thrusters. The opportunity for substantial improvement of confidence in theoretical modeling of coaxial devices (vs rectangular arrangements) encourages a focus for future development of PPTs in the direction of coaxial devices. Maintenance of connection to the flight experience of traditional systems represents the major challenge to such development.

A Micro-PPT developed by Spanjers represents a particular form of coaxial PPT. Basically, a high-voltage pulse delivered to the exposed end of a coaxial cable provides the ablation arc without requiring a separate igniter and circuitry. The relatively low energy of operation permits this simplification, and correlates well with application to Micro-Sats (*S/C* mass <20 kg). The present Micro-PPT package has a mass of less than 0.5

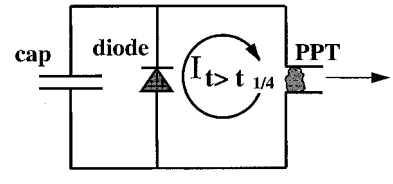

Fig. 11 PPT circuit with diode to prevent current reversal in the thruster.

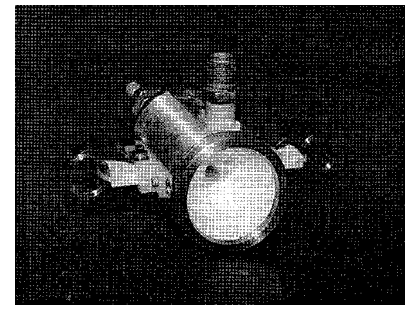

Fig. 12 Coaxial side-fed PPT with power cable and side-mounted igniter plug.

kg, and uses a discharge energy of 0.8 J to generate impulse-bits of about 2 μN-s.

Guman and Peko[17] investigated a breech-fed coaxial PPT (Fig. 13) with a central anode having a retaining shoulder and an axial spring. The I_{sp} was found to vary with the stored energy and ablated mass as $I_{sp} \sim (E_0/m)^{0.78}$, and it was concluded that the thruster mechanism was partly electromagnetic [$I_{sp} \sim (E_0/m)^{1.0}$] and partly gasdynamic [$I_{sp} \sim (E/m)^{0.5}$]. Increasing the nozzle size and decreasing the stored energy tended to decrease I_{sp}.

The University of Illinois coaxial thruster design (PPT-3, PPT-4),[66,67] like the Zond-2, is characterized by a relatively high value of impulse bit per joule, low specific impulse, and a predominantly electrothermal acceleration mechanism (Fig. 12). The thruster is side-fed, and employs a high area-ratio ceramic nozzle to extract as much gasdynamic and electromagnetic thrust as possible. The single igniter plug is located in the nozzle, between the exit and the throat. The bulk of the stored energy is delivered to a small-diameter propellant-lined cavity, closed at one end by the anode, with a large ratio of length to diameter, minimizing plasma heat loss to electrodes and insulators, and producing pressures on the order of 50 atm from ~10 J. The current pulse is nonreversing because of the

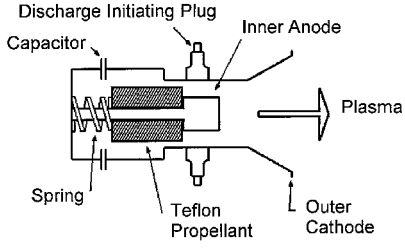

Fig. 13 Coaxial solid-propellant thruster schematic.

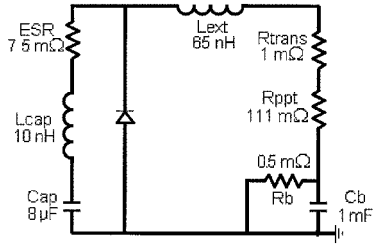

Fig. 14 Fixed LRC circuit model of PPT-4 thruster.

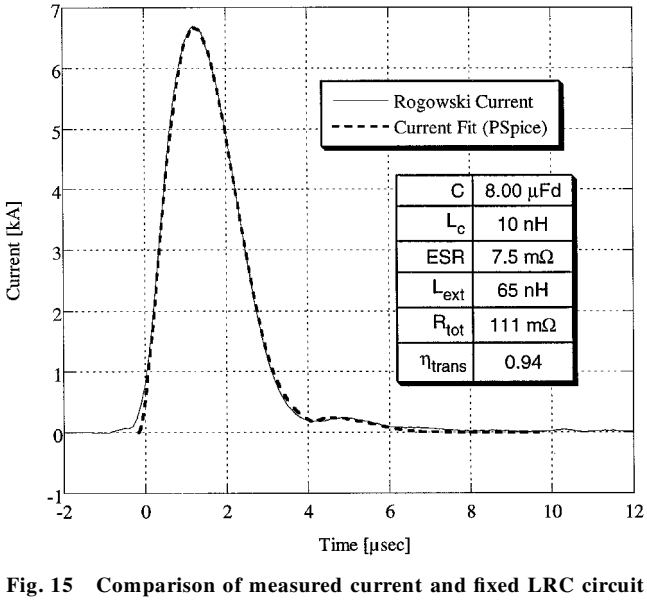

Fig. 15 Comparison of measured current and fixed LRC circuit model current for PPT-4 thruster.

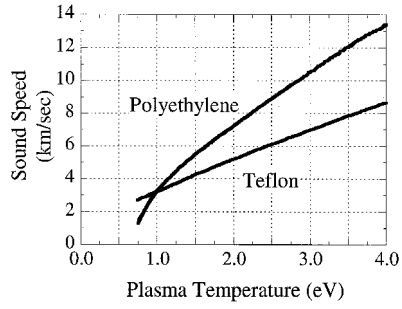

Fig. 16 Equilibrium plasma sound speed vs temperature predicted by the Sesame code.

use of a diode across the capacitor, and the pulse length is short compared to the characteristic acoustic time L/a (length/sound speed), such that the stored energy is delivered and the electromagnetic thrust is produced prior to most of the gasdynamic thrust. The PPT-4 current pulse is modeled accurately with a fixed LRC circuit (Figs. 14 and 15).

The electromagnetic thrust component of the PPT-3/PPT-4 coaxial thrusters is $\frac{1}{2}L' \int I^2\,dt$, where L' is 0.66 μH/m, about 72% that of the LES-6 rectangular thruster (Appendix A). The gasdynamic component can be approximated by assuming that the stored energy E is delivered to the subsonic cavity, of volume $L \times A$, in an adiabatic, constant-volume process, giving a pressure $p = (\gamma - 1)E/LA$. The impulse bit per joule is then

$$\frac{\int T\,dt}{J} \cong \frac{\frac{pAL}{a}}{E} \cong \frac{\gamma - 1}{a} \tag{7}$$

The temperature, γ, and sound speed, a, are typically 1.5 eV, 1.3, and 4 km/s from the thruster resistance and the Sesame code (Fig. 16), giving 75 μN-s/J. The measured value is 60 μN-s/J (Fig. 8), corresponding to a heat loss of 20% in the capacitor and cavity. The specific impulse is 600 s, corresponding to a velocity 50% higher than the sound speed. The gasdynamic thrust contribution can be decreased and the electromagnetic component increased by operating at higher temperature.

VII. Alternative Propellants

A large number of propellants have been evaluated in the hopes of finding improvements over Teflon. The evaluations are usually performed by measuring thrust stand performance, and by examining the posttest condition of the ablated surface.

Guman[25] measured performance on a breech-fed PPT for Teflon and other plastics, including Kynar®, Viton®, Fluorel®, Kel-F®, Genetron®, Halon®, Delrin®, CTFE-2300®, polypropylene, and polyethylene. Additives for Teflon such as lithium hydride to reduce the ionization potential were proposed. Preliminary performance tests showed that three of the plastics tested, polypropylene, Delrin-AF®, and Kynar®, formed surface char. The other propellants showed variations in I_{sp} from 947 s (Kel-F) to 2410 s (polyethylene) with Teflon at 1085 s in a breech-fed configuration.

Palumbo and Guman[41] evaluated several commercial plastics (Celcon®, Halar®, Tefzel®, and Halon) as well as Teflon doped with 10 and 30% $InBr_3$, at 400 J. Although it was concluded that the performance of these plastics was lower than that of Teflon, the tests were only run in the breech-fed mode, preventing direct comparison with the side-fed mode. Palumbo and Guman[59] also attempted to evaluate Teflon seeded with alkali metals, but the sintering temperature of the Teflon was above the metal melt temperature. An attempt was made to use a propellant composed of 80% LiH, 20% polyethylene, but the lithium melted out on the surface and very low values of ablated mass were achieved. It was concluded that, to be suc-

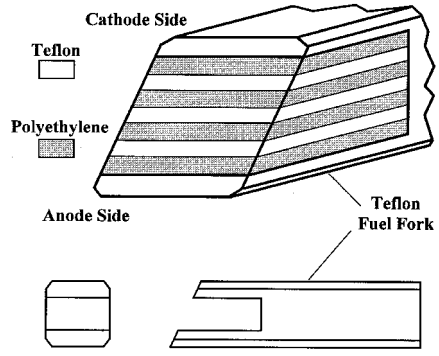

Fig. 17 Fuel geometry, showing Teflon/polyethylene laminations.

cessful, any additive would have to decompose at about the depolymerization temperature of Teflon (330°C).

NASA Lewis Research Center and Ohio State University,[68] using an LES-8/9 series thruster, performed experiments to alter the ablating surface of the propellant bar by alternating layers of Teflon with new propellant materials. This technique, it was hoped, would provide improved specific impulse without losing the overall dielectric strength of a pure Teflon surface. Figure 17 depicts the arrangement of lamina of different materials in the modified propellant bar. Earlier attempts to use plastics such as polyethylene, aimed at lowering the molecular weight of exhaust products by eliminating fluorine, failed when severe carbonization ("charring") occurred.[69] In the recent experiments, laminates of Teflon ($[C_2F_4]_x$) and polyethylene ($[C_2H_4]_x$) of several different thicknesses were tested. All cases displayed the tendency for the polyethylene surfaces to carbonize, while the intervening Teflon receded at a faster rate. Such modification of the surface occurred over several thousand firings and did not affect the ability of the combined surface to hold off the initial charging-voltage, because merging of carbonized layers across the intervening Teflon did not occur. Comparison of the properties of Teflon and polyethylene suggests that the quest for improved PPT propellants may depend on subtle features, such as the thermal diffusivity and the temperature for polymer decomposition.[68]

VIII. PPT System Heating

Concern for the effects of propellant temperature on PPT performance led to two experimental efforts aimed at monitoring temperature values within the propellant and at other stations in the PPT. As part of a thorough experimental effort to analyze PPT behavior, Spanjers et al.[70] placed a series of thermocouples at several locations within the Teflon propellant bar. Higher mass loss during PPT operation correlated with higher temperatures at higher average-power levels. Mass loss at very low speeds by evaporation between discharges, in addition to macroparticle generation, can significantly reduce PPT performance. Similar experimental work by Kamhawi and Turchi[71] had been prompted by MACH2 calculations, which correctly predicted the impulse-bit because of discharge, but required late-time material loss to account for the mass loss per shot in LES-6. In these experiments,[71] thermocouples were placed in the Teflon propellant and in both electrodes of a breech-fed rectangular PPT.[72]

In both experimental efforts, the size of the thermocouples limited the spatial and temporal resolution of the measurements. Thus, the temperature values obtained represented average values over times much longer than the discharge time, at distances of a millimeter and more from the propellant face. Over the course of the first thousands of shots, temperatures rose in all cases, approaching plateau values that depend on heat transfer from the PPT to the rest of the experimental apparatus. The anode is the highest temperature element. Elevated temperatures of the electrodes leads to concerns with heat transfer to the capacitor as part of the overall thermal design of the PPT. The increase of operating temperature with power suggests that PPT design and performance, in terms of capacitor lifetime, allowable charging-voltage, and mass ablation will depend on the mission application, e.g., station-keeping vs orbit raising.

IX. Additional System Issues

With a long history of flight application, the PPT should have bright prospects for further use in space. For each new PPT mission, however, questions persist regarding electromagnetic interference (EMI) and contamination of the spacecraft by the PPT exhaust. EMI must always be addressed in a new spacecraft because of the general trend toward more capable, but often "softer" electronic subsystems. Contamination by the PPT thruster must be considered even though PPT thrusters eject less mass than chemical thrusters because of the possibility of carbon deposition.

In the rectangular form of the traditional PPT design, the basic current loop of the plasma discharge acts as an excellent antenna. In principle, external coils may cancel this broadcast, at least partially, but most designs pay little attention to such matters. Plasma discharges also can provide electromagnetic emissions by subtler processes. Thomassen[72] measured radiation in the 0.2–18 GHz band from a LES-8/9 thruster using a broadband antenna. Radiation was only observed during the first 0.5–1 μs of the 8-μs discharge pulse, during the high-voltage breakdown phase, and was characterized by a flat frequency spectrum with a total radiated power of a few hundred milliwatts over the frequency range, compared to a discharge power dissipation of 10 MW.

Extensive EMI tests and corrective measures were performed by Ebert et al.[2] on the NOVA Spacecraft. A highly detailed account of test and shielding methods used during flight qualification is described.

Coaxial geometry provides a simple approach to reducing potential EMI concerns with PPTs. Spacecraft designers must then confront the difficulty of accepting a device that looks different than the one previously selected by other designers. Certainly, the burden rests with the thruster engineers to demonstrate the performance and lifetime of a coaxial PPT, including subtle differences in propellant handling and ignition.

Historically, PPT effluents have not compromised spacecraft operations, although the use of Teflon as the propellant offers an exhaust consisting of various forms of carbon and fluorine, mostly ions of both species. Production of macroparticles and late-time evaporation of propellant provides molecular and macromolecular constituents that might trouble the spacecraft environment, and electrode, sidewall, and igniter material may also appear in the exhaust. Erosion of thruster components may also contribute to contamination (but at much lower mass flow rates).

For flight-qualified PPTs, electrode and insulator erosion has not proven to be a life-limiting issue, principally because of the relatively large ablated mass. Erosion can become important if the specific impulse is too high, in which case the ablated mass can be insufficient to provide current carriers to the discharge. In this situation, which can happen in a PPT for $I_{sp} > 3000$, the discharge will seek charge carriers from the electrode and insulator material. Results for PPTs operating at very high I_{sp} must therefore be viewed with caution.

The issue of spacecraft contamination by electric thruster exhaust can be examined experimentally and by numerical plume modeling. Experimental measurements are performed in cryogenically cooled or large-diameter vacuum facilities to minimize tank wall effects, and numerical methods employ collisionless particle-in-cell and Monte Carlo collision techniques.[73] Although PPT exhaust contamination has not been a spacecraft problem for attitude control applications,[4] both forward flow and backflow contamination can be a concern for high-power PPTs or for applications involving sensitive diagnostics, e.g., optics.

Backflow contamination was measured for the Millipound PPT[74] using both a Faraday cup and a liquid nitrogen-cooled quartz crystal microbalance (QCM) near the exit plane at radial distances up to 1 m from the thrust axis. These measurements were supported by photography of the luminous plume, which slowed a plume expansion half-angle of 40 deg, associated with the charged particles. The Faraday cup diagnostic confirmed that the backflow was predominantly electrically neutral, at most 5% ionized. The QCM was used to measure backflow mass flux, which decreased with radius out to 70 cm from the axis. A modified nozzle with a shield plate reduced the backflow by about a factor of 2.

Extensive contamination measurements for both forward and backflow mass flux were made on an LES-8/9 PPT, using langmuir electrostatic probes and quartz wafers.[75] In the forward direction, a base film was deposited with imbedded 1- and 5-μm particles. The deposition material was composed of carbon, fluorine, and a few 5-μm particles of electrode material, and was found to decrease rapidly beyond 50-deg off-axis. In the back direction, no measurable deposition was measured after 2×10^5 pulses. It was concluded that "... to first order, spacecraft surfaces behind the PPT should not be significantly contaminated by thruster exhaust products."

Electrode studies were performed by weighing the electrode mass loss after 9000 discharges.[59] Two distinctive conclusions were reached. Using the same material for the cathode and anode, the anode erosion was typically 10 times that of the cathode. Secondly, a copper anode was observed to erode one-tenth as much as stainless steel under similar conditions.

X. Velocity and Related Plume Measurements

More than any other measurement, velocity displays the complexity of the PPT acceleration process. It was discovered at an early stage that a broad velocity distribution was present in the PPT exhaust, with data from older experiments repeatedly indicating a correlation of higher speeds with higher ionization states. The notion of accelerating ions of different charge states in the same electric field thus readily suggests itself.

This interpretation, however, cannot apply if the current density distribution (in which the Hall electric field resides) extends over a streamwise distance much larger than the mean free paths for momentum transfer collisions among the various species. Furthermore, up to four charge-states, e.g., C to C^{+++}, would have to coexist in comparable proportions at the same time and position for subsequent acceleration by the Hall field. However, ionized gases typically offer one charge-state that dominates, with relatively small populations at the next higher and lower levels. This would seem to lead to alternative explanations for the observed range of velocities, such as the tendency to create higher charge-states in the lower density, higher-speed portions of the PPT exhaust.

At this time, interpretation of the velocity data in PPT experiments remains an open issue. The difficulty of such interpretation increases when experimental conclusions presented by various authors receive critical examination. For example, spectroscopic observation of the unsteady and nonuniform plasma flow in PPTs can introduce errors because of sampling quite different plasmas along the optical path. These errors include erroneous values of electron temperatures from perceived line-intensity ratios, and overestimates of heavy-particle temperature when line-broadening measurements capture unsteady components of directed velocity, turbulence, and collisional effects. Furthermore, time-variations of plasma chemistry and luminosity may incorrectly suggest convection. Use of probes such as Faraday cups in the transient, hypersonic flow of a PPT also invites difficulties of interpretation, leading perhaps to curious conclusions, such as a low degree of ionization combined with a high charge-state. With these caveats, we review the experimental velocity results for PPTs.

Vondra et al.[76] measured plasma velocity in the plume of the LES-6 breech-fed thruster by two techniques. The mass-averaged velocity from the specific impulse was 3.2 km/s. Image converter images of the luminous front showed a luminous plasma on the Teflon surface during the pulse, and a high velocity plasma with an initial velocity of 11 km/s during the first current half-cycle, followed by an increase to 32 km/s (10 times the mass-averaged velocity) for the remainder of the pulse. The velocity increase occurred shortly after the peak in electromagnetic force, when 75% of the capacitor energy had been discharged. Plasma velocity measured with a Faraday cup was 42.5 km/s, and was presumed to be C^{+++} and F^{+++} ions. The total charge collected by the cup implied a 10% ionized plasma. Electron density in the discharge from laser interferometry was $\sim 2 \times 10^{22}$ m^{-3} and the electron temperature from emission spectroscopy of C lines was 3–8 eV. Interestingly, the inferred ion temperature from line broadening was 10–15 eV, double the electron temperature.

Doppler measurements of individual species showed higher velocity for more highly ionized species, as given in Table 4. It was concluded that the high-velocity species, comprising 3% of the mass, contained 15% of the stored energy.

Similar velocities, 30–35 km/s, were measured by Guman[77] on the LES-6 thruster for doubly and triply ionized C and F, by observing the time of arrival of spectral lines. Singly ionized C and F moved at about two-thirds the velocity of the multiply ionized species. Neutrals were observed at 5–15 km/s, significantly faster than the mass-average velocity of 3 km/s. It was concluded that it is inappropriate to speak of a single exhaust velocity for the PPT.

From the LES-6 velocity data[78] (Table 4) the bulk of the exhaust kinetic energy and momentum was found to reside in the charged particles (about 10% of the ablated mass, based on Faraday cup measurements). The authors propose that the fastest particles are accelerated early in the pulse, and the slower particles later, under conditions of higher pressure and lower temperatures.

The plasma velocity in the Russian MIPD-3, discussed earlier,[57] was measured four ways: traversing spatially in the plume with emission spectroscopy; laser interferometry; langmuir probe; and magnetic probes. The velocity of C^+ and F^+ ions was found to be 35 km/s by spectrometry. With interferometry a fast ion blob at 25–35 km/s was observed, followed by a slower blob at 13–15 km/s, both faster than the mean velocity of 11 km/s. Velocity of the neutrals was measured as 15 km/s by spectroscopy. With an electrostatic probe the fast ions were 30–35 km/s, followed by slower ions at 14–16 km/s. The same probe detected $\sim 2 \times 10^{16}$ electrons/cm^3 in the arc, at a temperature of 1.8–2.6 eV, invariant during the pulse. During the first half-cycle the magnetic probes showed no current at the back insulator of this side-fed thruster and a $\boldsymbol{j} \times \boldsymbol{B}$ current front moving in the flow direction at 20–25 km/s.

The velocity of the exhaust gas in a Japanese PPT[47] was also analyzed with electrostatic time-of-flight probes, located 107 and 202 cm from the thruster. The measured ion flow velocity was 34 km/s with this method. From a total energy

Table 4 LES-6 species velocities from Doppler measurements

Species	Velocity, km/s
C	10 ± 5
C^+	25 ± 5
C^{++}	——
C^{+++}	35 ± 5
F	10 ± 5
F^+	20 ± 5
F^{++}	——
F^{+++}	30 ± 5

argument it was concluded that the bulk of the flow consisted of neutrals moving at a much lower speed.

Thomassen and Tong[79] used a multiple-pass He–Ne laser interferometer and Faraday cup to measure the spatial and time dependence of the electron density in the Teflon discharge plasma, 1–26 mm in front of the ablating surface. The total charge measured by the Faraday cup indicated that the plasma was 40% ionized 3.5 mm from the ablating surface, decreasing to 18% ionized at 16 mm. Assuming the exhaust gas to be a drifting, expanding Maxwellian with thermal velocity v_T and drift velocity v_0, curve fits to the interferometer density data gave v_T = 9.3 k/s and v_0 = 27.9 km/s. This thermal velocity can be compared to the Teflon equilibrium sound speed given in Sec. XI (Fig. 16). Using the resulting density and ion temperature (7.6 eV) to predict the pressure, they concluded that the gasdynamic forces contribute 48% of the thrust, and the magnetic forces contribute 52%.

Hirata and Murakami[47] performed mass spectrometer (MS) measurements in a vacuum chamber on the residual exhaust gas from the Japanese PPT flown on their Engineering Test Satellite IV.[80] The thruster energy was 2.6 J at 3 pulses/s, and 10 μg was ablated per pulse. Although the measurement was not time-resolved, the calculated time for three-body recombination was very long compared to the mean chamber residence time, and the MS readings were therefore thought to be characteristic of the molecular spectrum of the exhaust gas. These showed a large peak corresponding to the CF molecule, and smaller peaks corresponding to C, F, CF_2, and CF_3. It was concluded that a considerable fraction of the Teflon was ejected as a high mass molecule, which could have happened late in the current pulse. The authors did not evaluate the possibility of wall recombination.

Spanjers et al.[81] investigated a thruster (XPPT-1) similar to the LES-8/9, but with better diagnostic access, and with axial instead of 30-deg-angled thrust. Time-resolved electron and neutral densities were measured with a HeNe laser interferometer. The laser beam was reflected three times parallel to the fuel rod at a distance of 8 mm from the face, creating a plasma path length of 7.5 cm, effectively measuring the change in index of refraction caused by the presence of plasma. Both neutral and electron density were found to vary linearly with energy over a range of 2–80 J, with the neutral density $n_n \sim$ few $\times 10^{16}$ cm^{-3}, about five times the maximum electron density. After adopting previous results for fast (40 km/s) and slow (3 km/s) velocity measurements,[78] it was concluded that for a 25-J discharge, the kinetic energy of the fast particles was 4.6 J, implying a thruster efficiency of nearly 19%.

In later work on the same thruster, electron density was easily detected early in time, falling to zero at approximately the end of the current pulse.[81] Neutral density was observed for times much longer than the end of the current pulse, and it was concluded that the neutral density was about four times the density of the ionized species. Late-time ablation of 300 m/s macroparticles, hypothesized to be thermally expelled Teflon erupting from the surface, was observed. Increasing the stored energy produced a proportional increase in ablated mass and in electron and neutral densities.

Using the same thruster, Markusic and Spores[82] studied the time-resolved spectral emission of a Teflon plume in the visible (350–750 nm) for a parallel-plate PPT. The capacitor energy was 15, 30, and 45 J, and the spectrum was resolved at the horizontal midplane either with a charge-coupled device array or for a predetermined spectral line with an exit slit and photodiode, for a time period up to 75 μs after termination of the current pulse. Species identified were F, F^+, C^+, C^{++} and C_2, but not C or CF, whose lines were outside the survey region. Plots of spectra normalized to the intensity of the 427 nm C^+ line were strikingly independent of stored energy, as was the electron temperature at peak current, determined by the relative intensity of C^+ excited states. The spatially averaged electron temperature was found to be 1.4 ± 0.2 eV in the arc. Velocity determination from propagation of the spatial distribution of C^+ emission gave 15 km/s, and unlike some observers, about the same value for C^{++} and F^+. These velocities, and those obtained concurrently by Doppler shift, also 15 km/s, were concluded to be low for reasons relating to specifics of the diagnostics.

Eckman et al.[83] made detailed plume measurements of ion velocity in the LES-8/9 thruster, and found that the ions traveled in a first wave at 35–55 km/s, and in a second wave at 28 km/s. They suggested either multiple ionization or the slug-restrike-steady-state mode of operation of Turchi and Mikellides[84] as a mechanism. Neutral velocity and density were measured with a fast (3-μs response) ionization gauge, with the assumption that the neutral temperature was equal to the Teflon surface temperature of 420 K. The density was found to be on the order of 10^{20}/m^3, and to decay slowly on a time scale of ~1 ms.

The complexity of plasma motions in the PPT includes the possibility of different charge states arising at different times, with quite different speeds because of either propagating or ablation-arc modes during the discharge pulse. When currents are no longer present, the PPT exhaust comprises hot plasma remaining from the discharge pulse, followed by colder material that leaves at much lower speed. Directions for improved performance therefore require guidance from theoretical modeling that can account properly for the variety of speeds and masses produced.

XI. Recent Advances in PPT Modeling

The problem of associating the mass evolved from the propellant surface with the impulse developed during the operating pulse represents the principal difficulty in establishing the performance of the PPT in terms of its specific impulse or (average) exhaust speed. Empirically, measurement of the total mass lost by the surface over many discharges provides the mass loss per shot. This value divided into the impulse per shot offers the average exhaust speed. Experimental data suggest that the mass loss is proportional to the stored energy (Fig. 9). This intuitively pleasant result implies a constant value for the average exhaust speed, and a reasonable way to scale new designs from existing data. At this level of discussion, however, there is no further insight to provide a firm basis for improving PPT performance.

It is necessary to develop theoretical modeling that can incorporate physical processes not captured by lumped-circuit representations and empirical scaling laws. For example, the discharge current must have the opportunity to flow both through paths propagating along the accelerator electrodes and through a path remaining near the propellant surface. This requires a formulation at least at the level of MHDs to obtain the distribution of current density within the thruster. An effort to extend PPT operation to the millipound level first attempted such an approach.[85] At the time, however, computational simulation of plasma acceleration was too difficult to achieve within a program largely devoted to experimental exploration and development. Over the past decade, the MACH2 code, created to support experiments with powerful plasma-guns,[86] has been applied to electromagnetic thruster problems. These applications included quasisteady MPD arcjets[87] and steady-state, applied-field MPD thrusters,[88] and more recently the PPTs.[84,89]

The MACH2 code calculates the behavior of unsteady, MHD flow in complex geometries. The flow may have two directions of variation and three directions for vector-field components. For example, MACH2 computes the unsteady evolution of all three components of magnetic field and flow velocity in the plane containing the axis of symmetry of an applied-field, MPD thruster. The code allows three temperatures (heavy-particle, electron, and radiation) and couples to the SESAME tables for composition, equation-of-state, and transport properties of many materials; ideal gas and classical

plasma options also exist. Faraday's law and a generalized Ohm's law (including the effects of Hall fields and electron pressure gradients) combine to compute magnetic convection and diffusion, based on the electrical resistivity of plasma in the presence of electric and magnetic fields. For situations of high current density and low particle density, options exist to invoke phenomenological models of anomalous resistivity because of microinstabilities. Options for anisotropic thermal conduction by both heavy particles and electrons in magnetic fields also exist. Choices for radiation transport include optically thin, equilibrium and nonequilibrium diffusion models.

The need for self-consistent addition of mass during the discharge pulse makes numerical simulation much more difficult for the PPT than for a gas-fed, plasma thruster. MACH2 was modified,[84,89] within its continuum formulation, to use the equilibrium vapor pressure of the propellant material [see Eq. (1), Sec. II)], based on the surface temperature, for the boundary value of pressure at the propellant surface. The normal algorithms in MACH2 then calculate the motion of vapor into the computational domain. A separate routine for two-dimensional, unsteady heat flow in the solid propellant iterates with MACH2 to compute the surface temperature in response to the net energy flux (conduction, radiation, and convection) from the plasma.

MACH2[84] provides the distributions of plasma discharge conditions, such as mass density, temperature, and current flow, as functions of position and time. Examination of these distributions permits delineation of physical mechanisms at a level of detail that remains beyond present diagnostic efforts. Comparison with available experimental data can provide some insight on PPT behavior offered by the relatively simple processes modeled by MACH2. For example, at various times and locations during the discharge pulse in LES-6, calculated plasma speeds range from nearly zero, adjacent to the propellant face, to values exceeding 35 km/s. Higher speeds correlate with regions of lower density and higher charge state. Experimental data (Sec. X) connecting higher speeds with higher charge-states might suggest substantial slip between species of different charge, a result at variance with estimates of collision mean-free-times. MACH2, which considers only a single-fluid in local thermodynamic equilibrium, instead indicates that the data could result simply from spatial and temporal variations of ionization in the accelerating flow.

As indicated in Fig. 18, these same calculations[84] for LES-6 captured both the magnitude and variation of the impulse-bit for the available values of experimental data. Such agreement must be considered somewhat fortuitous, the result of compensating errors, because of several limitations. These include the use of a two-dimensional calculation (in the plane of the current flow) for a three-dimensional problem, and approximate formulations for plasma composition and transport coefficients. The calculated value of mass ablated during the discharge pulse is less than the experimental value by about an order of magnitude. This disagreement led to speculation that most of the propellant mass evolved after completion of the current pulse as the surface cooled between firings.[51] Such late-time evolution could also explain the experimental observations of flow speeds greatly exceeding the average exhaust speed as represented by the specific impulse. Calculations extended to estimates of the base temperature of the propellant necessary to account for the mass loss at low speed and the consequences of such mass loss on PPT performance.[51] The question of propellant temperature led to closer experimental examination of PPT system temperatures (Sec. VIII).

In addition to numerical simulations, the behavior of a PPT has been modeled analytically as a quasisteady, ablation-fed thruster.[24] This model invokes a magnetosonic condition as the flow exits the ablation-arc. The pressure and temperature near the surface then assume values that provide the mass flow needed to support the magnetic pressure gradient across the discharge. Larger differences in magnetic pressure, i.e., higher currents in a given width, demand higher mass flow rates (for an exhaust speed that remains rather constant). This means higher values of the equilibrium vapor pressure at the surface and higher values of surface temperature. For pulsed heat conduction in the solid propellant, the total heat delivered to the propellant scales with the surface temperature. The surface, therefore, tends to remain at elevated temperatures for longer times after the discharge pulse, evaporating more material without the benefit of electromagnetic acceleration. The ratio of material evolved after the discharge pulse to that created during the pulse tends to a constant on the order of five. The analytic model suggests that by allowing the current pulse to decline gradually as the propellant surface cools, electromagnetic acceleration to high speed might continue, thereby decreasing this ratio.

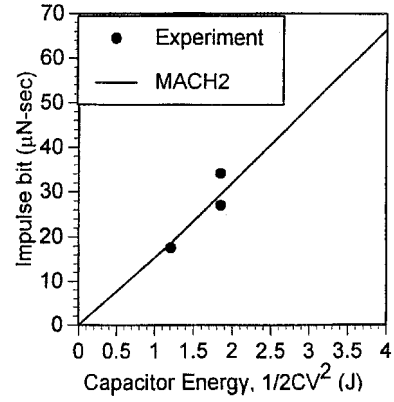

Fig. 18 Comparison of impulse bit predicted by the MACH2 code with experiment.

Higher surface temperatures during the discharge also permit decomposition or phase change at greater depth in the solid propellant. The resulting ejection of low-speed macroparticles could burden both the specific impulse and thrust efficiency of the PPT, as well as increasing concern for spacecraft contamination.

Accurate values for the plasma composition and transport coefficients remain critical for detailed simulation of the PPT. For equilibrium plasmas the Los Alamos Sesame code is available to predict global thermodynamic and transport properties such as enthalpy, entropy, mean charge state, electrical conductivity, and sound speed.[90] A Sesame code prediction of the latter for Teflon and polyethylene is shown in Fig. 16. For nonequilibrium PPT plasmas, the decomposition of a polymer such as Teflon into constituent atoms and molecules, and the subsequent creation of various ionized species certainly represents a formidable process to analyze, even without the interplay with a MHD flowfield. Some progress occurred recently with the completion of a model for Teflon in two-temperature (heavy-particle and electron), local thermodynamic equilibrium.[91] This model incorporates 25 species, and allows a parametric variation of equilibrium between vibrational states and the translational states of either electrons or heavy particles. Figure 19 displays the predicted partial pressures of F and F^+ in a Teflon plasma for the indicated values of heavy particle and electron temperatures and total plasma pressures. This model now provides the basis for calculation of transport properties in a Teflon-fueled, PPT discharge. The continuum, LTE nature of the model clearly becomes inappropriate in the lower-density, higher-speed regions of the flow. Comparison of results from MHD code simulations using this model with limited analysis based on kinetic theory can then allow assessment of the importance of the two-temperature, LTE approximation in different regimes of PPT operation.

Consideration of noncontinuum flow processes requires theoretical techniques beyond MHD codes. For example, numer-

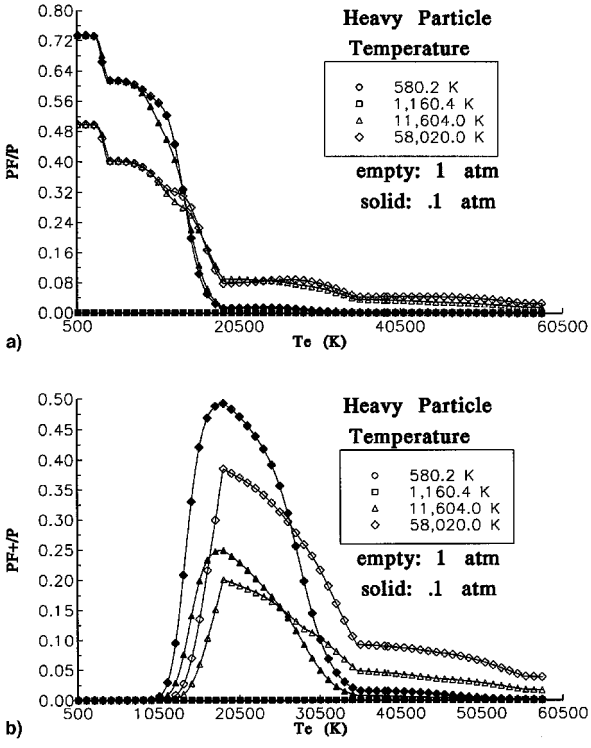

Fig. 19 Two-temperature code-predicted partial pressure of a) F and b) F^+ in a Teflon plasma.

ical modeling of PPT exhausts,[92] using combinations of direct-simulation Monte Carlo (DSMC) and hybrid particle/fluid techniques, may help to quantify conditions in the PPT plume, at least for gaseous constituents. Such calculations have already received input data from MACH2 calculations, but further work is needed to handle the possibility of significant magnetic energy in the flow when the continuum approximation fails.

XII. Electrical Circuit Developments

Substantial swings in the capacitor voltage associated with the oscillating, reversing waveform in the usual PPT circuitry exacerbate a principal design difficulty: capacitor lifetime at high-energy density. The energy-storage capacitor represents a major portion of the dry-mass of the PPT, and the primary determinant of the specific power of the thruster system. Optimization of electric thrusters often depends on the product of specific power (W/kg) and the thrust duration (s). For pulsed thrusters, such as the PPT, this product equals the product of specific energy (J/kg) and the number of firings during the mission. The specific energy of the capacitor and the capacitor pulse lifetime limit the value of the latter product. For high-voltage energy-storage capacitors, lifetime tends to scale inversely as charging voltage to a high power, e.g., V^{-7}, and also decreases strongly with the total, peak-to-peak voltage reversal experienced during an oscillatory waveform. The lifetime of the capacitor diminishes further by operating at temperatures above manufacturer's specification.

Although the experience with respect to capacitor life for the Millipound Thruster was very poor, capacitor development progressed in other fields to the benefit of the PPT. In the early 1970s, the General Electric company developed a low-loss capacitor for the Stanford Linear Accelerator (SLAC), which pulses at 180 Hz and has since accumulated over 25 years of operation. Commercial versions of this capacitor with 2–3 J storage and an equivalent series resistance (ESR) of ~30 mΩ are available for PPT applications. At total energies of 50 J, corresponding to a power of 50 W at a time between pulses of 1 s, the ESR of the capacitors in parallel would become less than the dynamic impedance of the PPT, even in a coaxial arrangement with a modest radius ratio. The concern with the value of the ESR relative to the total circuit derives from its effect on circuit efficiency and the decrease of capacitor lifetime with higher temperature caused by internal heating.

The oscillatory behavior of the discharge in the traditional PPT demonstrates the impedance mismatch between the LRC circuit and the PPT, indicating poor efficiency for electrical energy transfer. This impedance mismatch arises from design constraints on the values of capacitance, inductance, and charging voltage. At energy levels of several joules, the PPT capacitance of 10–30 μf combines with circuit inductances exceeding 50–100 nH to provide an impedance for critical damping much greater than the PPT impedance. Attempts to design a pulse forming network (PFN) with an impedance matching that of the PPT succeed at hundreds of joules,[11,49] but fail at a few joules because of the parasitic inductances.

To avoid the difficulty of PFN design, a different circuit was proposed and operated.[93] A two-step process of transfer energy from the capacitor to an inductive store, followed by energy transfer from the inductor to the PPT. During the second step (slightly after peak current), a second PPT fires, shortly after the capacitor voltage reverses. The second PPT serves as a so-called "crowbar" switch on the capacitor, restricting the voltage level to which the capacitor can recharge. This plasma crowbar switch can literally operate as a second PPT, ignited by a separate igniter or by plasma from the first PPT (Fig. 20). In the most recent arrangements, it has become integral with the first PPT, and fires automatically when the capacitor voltage reverses. Although the current waveform (Fig. 21) no longer has the constancy of a PFN-driven system, values of component capacitance and inductance readily match design needs. Recent theoretical work[24] suggests that a current waveform that declined roughly exponentially with time would provide electromagnetic acceleration of propellant evaporated as the surface cools late in the pulse. Extension of the pulse time permits the design of quasisteady, two-dimensional channel-flows,[49] which may offer additional improvements in PPT efficiency.

Solid-state diodes installed in parallel with the capacitor may offer more convenience than a plasma crowbar switch. A technique for preventing current reversal was achieved by Kimura et al.,[58] by inserting diodes in parallel with the capacitors in a 6-J capacitor bank. The diodes eliminated current oscillations in an attempt to enhance the effect of a transverse applied field

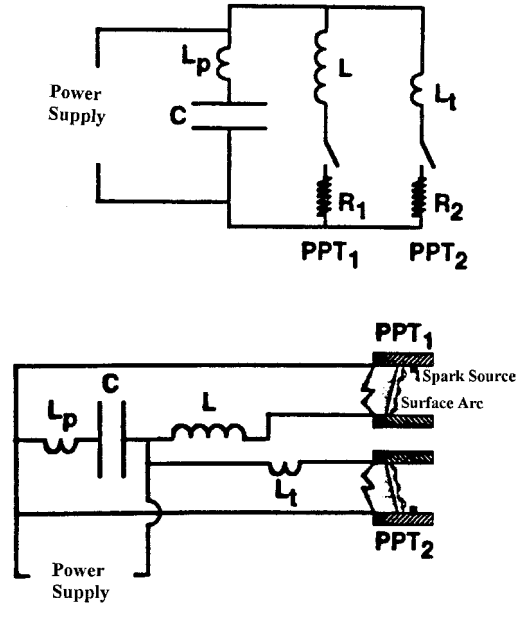

Fig. 20 Use of two PPTs to inductively store energy and produce nonreversing current.

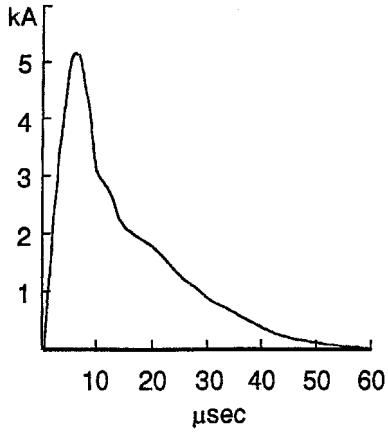

Fig. 21 Nonreversing current produced by two PPTs in an inductive storage circuit.

on the force. They were found to decrease the impulse bit about 10% with zero applied transverse field, and were not used with finite applied field. A diode has also been used on a 10-J coaxial PPT to prevent PPT current reversal, enhancing capacitor life.[66,67] The improved life afforded the capacitor, either by the diode technique or by a plasma crowbar switch, can also allow expanded design flexibility for higher-energy density and higher-temperature operation of the capacitor.

Additional improvements to the electrical circuitry of the PPT have been achieved by the substitution of modern electronic components in the charging system and the spark-plug ignition system. Thus, for example, the EO-1 thruster incorporates improvements over the LES 8/9 system by factors of more than 2 in weight and volume for the electrical circuits.[11] Further improvements in circuitry and components, e.g., energy storage, are highly desirable to increase the potential of the PPT.

XIII. Prospects for the Future

The next flight opportunity for the PPT occurs in 1999 on the EO-1 satellite.[11] Near the end of the mission, software will disable the pitch-axis wheel, and a breech-fed PPT will take over for three days, (corresponding to about 200,000 shots). The stored energy will vary from 5 to 40 J, and the impulse-bit from 100 to 700 μN-s, at a specific impulse of about 1100 s.[11] The proposed Deep Space 3 mission under NASA's New Millennium Program for "exoplanet" imaging and spectroscopy outside the solar system represents an opportunity for actual mission use of PPTs. This use occurs in two modes: spreading out the three spacecraft ("aperture filling") by a set of fire, coast and fire sequences; and stationkeeping and attitude control of the deployed array. The mission may use up to 12 PPTs per satellite, although different designs allow various degrees of component sharing. Each PPT would have an impulse-bit of 50 μN-s, and fire up to 25 million times.[14]

While these missions can be performed with PPTs of the traditional design, several areas of improvement offer the prospect of greater opportunity for PPT application. These areas include enhanced capacitor life, higher thrust efficiency, and higher specific impulse. The first of these derives from the use of inductive storage circuits (Sec. XII) that substantially reduce the level of voltage reversal on the capacitor. Improved capacitor design also helps by reducing losses in the capacitor, thereby reducing internal heating and increasing the electrical efficiency of the circuit. In mission analyses, the needed velocity change determines the necessary product of thrust efficiency, specific power, and thrust time. To the extent that the capacitor mass dominates the power system for the PPT, the product of the last two factors equals the product of specific energy of the capacitor and the number of firings allowed for its mission life. Thus, improving the specific energy of the capacitor and increasing its life, by reducing voltage reversals and operating temperature, combine to expand the range of velocity changes accessible with the PPT. Such improvement does not depend closely on the details of the plasma dynamics within a PPT.

To improve the PPT in terms of its actual behavior, we have to understand the several facets of plasma motion and mass evolution. In particular, at least two main components appear to exist in most PPTs: a fast component associated with processes during the discharge pulse, and a slow component resulting from thermal expansion of material without the benefit of electromagnetic acceleration. The former component may include contributions by both magnetic and gasdynamic pressure gradients in the discharge flow. The latter may comprise a prompt component because of plasma heated during the discharge, and a late-time portion related to the evolution of mass from surfaces heated by the discharge. Speeds in the fast component, which may correspond to either propagating or ablation-arc modes, can exceed 30 km/s in both experiments and MHD calculations. The slow component should scale with thermal speeds based on temperatures that range from the base temperature between firings (>370 K) to the plasma temperature at the end of the discharge pulse (~3 eV). For Teflon, these speeds would range from about 300 m/s (for C_2F_4) to about 7.8 km/s (for C).

The performance of a PPT in terms of efficiency and specific impulse depends on the masses associated with these very different speeds. Clearly, an efficiency proportional to the square of the impulse-bit divided by the mass loss per shot, while possibly useful for some system calculations, has no utility in guiding improvements based on detailed plasma dynamics. Indeed, the rather low value for specific impulse of some devices compared to values associated with measured flow speeds suggests that most of the mass in these cases corresponds to the slow component. This correlates well with estimates of the ratio of masses for the slow vs fast components of 5–10, from the analytical modeling[24] and MACH2 simulations of LES-6,[84] respectively.

Frozen flow loss represents a principal deficiency in most plasma thrusters, but is the cost of achieving higher specific impulse through an electrically active working fluid. This cost can be amortized by operating at a high exhaust speed. Higher thrust efficiency increases the value of velocity change accessible for an available product of specific energy and lifetime. Thus, increasing the relative mass of the fast component represents a useful direction for PPT improvement. Equivalently, the mass that escapes without the benefit of the electrical processes in the discharge should be minimized. The heat deposited in the propellant surface, however, will always cause material loss for some time. A solution,[24] therefore, consists of maintaining the electrical discharge as the surface cools.

In the near future, we may expect that understanding of the physical possibilities in ablation-fed, PPTs will overcome limitations that have remained unresolved after many years of empirical studies. Progress in the past was accomplished in an empirical fashion. (For example, as with the automobile engine, detailed understanding of the spark plug was not required to develop a practical system.) Future improvements will demand quantitative comparison of experiments and theoretical models. Much of our potential understanding of the PPT has been limited by the complexity of the discharge flowfield. With present experimental and numerical tools, only coaxial systems will allow such comparison. Extension of the long flight history of the PPT to future applications will, therefore, most likely combine nonreversing inductive circuitry with coaxial electrodes and nozzles.

Appendix A: Theoretical Formulations for Electromagnetic Forces in the PPT

The ability of the PPT to achieve exhaust speeds corresponding to kinetic energies a hundred times higher than elec-

tron temperatures in the plasma emphasizes the dominant role of electromagnetic forces in PPT operation. These forces are merely components of the Lorentz force density in the plasma

$$\boldsymbol{F}_d = \boldsymbol{j} \times \boldsymbol{B} \tag{A1}$$

where $\boldsymbol{j}$ is the local current density, and $\boldsymbol{B}$ is the local magnetic field. Integration of the axial component of the force density over the volume of the plasma provides the total electromagnetic contribution to the thrust. Figure 4 displays a sketch of the basic geometry of the current flow and magnetic field in the PPT. In rectangular form, the discharge has length h, width w, thickness μ, and an instantaneous position, z, downstream of the return conductor. Two approaches to integrating Eq. (A1) permit calculation of most of the electromagnetic contribution to thrust without needing to know this current distribution. The field-theoretical approach works directly with the magnetic field distributions in the PPT, whereas the circuit-theoretical approach uses the intermediary of inductance formulas to deal with a magnetic field distribution whose magnitude scales with the circuit current.

Field-Theoretical Approach

By replacing the current density with the curl of the local magnetic field, the force density appears in terms of a gradient of the magnetic pressure, $B^2/2\mu$, and the so-called "magnetic tension," $-B^2\boldsymbol{r}/\mu r^2$

$$\boldsymbol{F}_d = -\nabla B^2/2\mu - B^2\boldsymbol{r}/\mu r^2 \tag{A2}$$

where $\boldsymbol{r}/r^2 = -(\boldsymbol{B}\cdot\nabla B)/B^2$ defines an effective radius of curvature of the magnetic field lines. The notion of magnetic pressure acting in the manner of gas pressure is always qualitatively useful in considering PPT behavior. Quantitative calculations using Eq. (A2) need computer assistance, except in special situations.

Circuit-Theoretical Approach

By avoiding the plasma, consideration of the external circuit offers some success, albeit with some loss of accuracy, in describing PPT behavior. The force in the plasma reacts against the currents traveling in the solid conductors of the PPT circuitry. Calculation of the net axial force acting on these conductors, therefore, also provides the electromagnetic thrust. Over much of the circuitry, this calculation merely requires knowledge of the variation of circuit inductance with displacement in the axial direction

$$\boldsymbol{F} = (J^2/2)\nabla L \tag{A3}$$

where J is the thruster current, and L is the thruster inductance. The axial component of electromagnetic force depends on the derivative of inductance with respect to the axial size of the circuit path (see Sec. III). The application of Eq. (A3) must proceed with caution if used where mutual inductances exist between portions of the current distribution.[16]

The virtue of the circuit approach to calculation of the electromagnetic thrust stems from the insensitivity of the result to changes in plasma discharge conditions. In coaxial PPTs, for example, variations of the insulator surface that leave the current distributions unchanged at the electrodes do not significantly alter the electromagnetic thrust. In rectangular geometry, however, the position of currents in the plasma determines the magnetic field at the circuit elements and the current distribution within these elements. Variations of thruster operation that affect the current distribution in the plasma, therefore, change the electromagnetic thrust as well.

Except in special cases, the current distribution in the circuit conductors does not satisfy the conditions of uniformity assumed by available inductance formulas. The actual distribution for a pulsed discharge requires a potential-theory solution based in part on the distributions of resistivity and velocity in the plasma. Thus, forces computed for three-dimensional arrangements using inductance formulas that assume fixed current-density distributions must be used with caution. Under some circumstances corresponding to the usual mode of PPT operation, the plasma discharge remains adjacent to the ablating surface of the propellant. If the current distribution within the plasma does not change with time, the integral of Eq. (A3) provides an excellent basis for computing the electromagnetic impulse.

The inductance of a closed circuit of rectangular conductors[94] is

$$L\,(\mu\mathrm{H}) = 0.4\left[\frac{3}{2}l + l\,\ell n\left(\frac{d}{b+c}\right) - d + 0.22(b+c)\right] \tag{A4}$$

so that

$$L' = 0.6 + 0.4\,\ell n\left(\frac{d}{b+c}\right),\ \mu\mathrm{H/m} \tag{A5}$$

For LES-6, $L' = 0.93$ μH/m, close to the curve-fit value of Solbes.[55]

A second approach to L' is the detailed calculation of Kerrisk[95] for parallel rectangular conductors, using the magnetic vector potential. The results for L' are interpolated from tables, or calculated from a curvefit equation. For the LES-6, this approach gives $L' = 0.871$ μH/m. These three methods average to 0.92 mH/m.

For more complex geometries, e.g., flared or diverging rectangular electrodes, L' would have to be calculated from the Kerrisk vector potential method, or from $IL' = \phi'$, where the flux gradient ϕ' is determined at the plane of symmetry from magnetic probe measurements.

For coaxial thrusters, the inductance gradient is readily calculated if the current density is axisymmetric. For thrusters with an annular electrode of radius r_a and a central electrode of radius r_c, the inductance gradient L' is determined by assuming azimuthal current symmetry and uniform axial current density to the central electrode. For this case L' is identical to that calculated for the MPD thruster[15]

$$L'\,(\mu\mathrm{H/m}) = \frac{\mu_0}{2\pi}\left(\ell n\,\frac{r_a}{r_c} + \frac{3}{4}\right) \tag{A6}$$

For the Illinois coaxial PPT,[66,97] $r_a/r_c = 12.8$ and $L' = 0.66$ μH/m, comparable to the value for a square PPT.

For a fixed circuit inductance, the square of the current amplitude will simply scale with the energy stored initially in the capacitor. Thus, impulse bit should vary linearly with energy per pulse. Figure 9 displays just such behavior, lending credence to the assumptions made in order to use Eq. (A3). For a linear variation of mass loss per shot as a function of stored energy, as suggested by Fig. 9, the PPT should have constant specific impulse. Experiments, however, indicate some variations of specific impulse and mass loss per joule of stored energy. Thus, these assumptions do not capture all of the physics of the PPT, and other electrical and thermal processes must play a role.

Thruster Dynamic Impedance

The traditional PPT uses a single capacitor to power the discharge, with current rising through the inductances of the external and thruster circuitry and opposed by resistances in the plasma and the external circuit, including the equivalent series resistance (ESR) of the capacitor. If the plasma path travels through a slug of material of given mass accelerated by the electromagnetic force [Eq. (A3)], two, first-order, ordinary differential equations provide the values of plasma position and speed. Motion of the current path with this plasma

introduces a resistance-like term, equal to the time derivative of the inductance, which modifies an otherwise standard LRC circuit. The position and speed of the plasma determines the instantaneous circuit-inductance and its time derivative. Solution of the differential equations for the circuit current and capacitor voltage completes the description of the electrical power pulse in the PPT.

Alternatives to the single-loop, slug description include models that fix the plasma discharge adjacent to the ablating propellant surface. The electric field in the plasma flow provides the load voltage seen by the external circuit. Analytic evaluation of this electric field, which includes both the resistive and electromotive terms, requires approximations and conditions, such as high magnetic Reynolds number and magnetosonic flow at the channel exit.[24] Attempts to combine both propagating and fixed current paths through the plasma can readily become rather ad hoc. Such combination achieves rigor when performed using a time-dependent, MHD analysis. This generally requires numerical solution by means of a code, such as MACH2.[24,84]

Appendix B: Thrust Stand Designs for PPT Performance Measurements

The two fundamental measurements made on a PPT are the thrust and the ablative mass loss. Because the time scale of the pulse is a few μs, time-resolved thrust and mass flow rate measurements are not possible, and the measurement must be made of the time-integrated thrust or "Impulse bit:" $I_{bit} = \int T\,dt$, typically several hundred micro-Newton-seconds. Thrust stand designs for impulse bit measurements are discussed next. Either a single pulse can be used as the basis for measurements, or the average thrust at a pulse rate N can be measured, giving $I_{bit} = T/N$.

The ablative mass measurements are made over a large number of pulses, say 1000, and the mass loss Δm per pulse is calculated from the measured total mass loss. This method then provides an accurate determination of the specific impulse from $I_{sp} = I_{bit}/g\Delta m$. From these two measurements an unambiguous PPT performance plot can then be made from I_{bit} vs I_{sp}.

A variety of thrust stand designs have been used for thrust measurements.

1) The Fairchild Industries vertical axis "swinging gate" thrust stand,[61] later used for MPD thruster measurements at Princeton University,[35,61] has a vertical swing axis with two torsional flexural pivots connecting a balance arm to a support frame. Arm displacement is measured by a linear variable differential transformer (LVDT),[61] a Bently-Nevada inductive sensor,[64] or by a laser interferometer proximeter system.[97] All of these can measure displacement in microns. Calibration is done by rolling a ball down a ramp or by an impact hammer.

2) A NASA Lewis Research Center's "inverted pendulum" thrust stand[98] can be used for high-energy (>100 J) PPTs. The device supports a platform with a stainless-steel foil flexure located below each corner, so that the pivoting axis is located below the center of mass, requiring the foil stiffness for stability. The thrust is measured either with an LVDT, or by stabilizing the platform with a feedback solenoid and measuring the current. Calibration of horizontal displacement is achieved by small weights on a flexible fiber run over a frictionless pulley to the platform.

3) A NASA Lewis Research Center's torsional type thrust stand[99] can measure low-energy PPT pulses, and is similar in principle to the Fairchild Industries thrust stand. The stand operates in single pulse or repetitive operation and is calibrated with an impact pendulum.

4) A GT-Devices, Inc., linear thrust stand[64,100] measured high-energy (~1 kJ) impulse bits for a single pulse, using a carriage on a linear rail with ball-bearing supports. Calibration was achieved by an impact pendulum using a focused laser and Ronchi ruling to produce a square wave signal from a photodiode.

5) The NASA Goddard Space Flight Center "MERTS"[101] thrust stand resolution was 20 μN, and was similar in concept to the Fairchild Industries design, using a differential capacitor displacement sensor. The stand was operated in a closed-loop (null-balance) mode, and was calibrated with an electromagnet.

6) PPT thrust on the 638-kg Japanese Engineering Test Satellite-IV was measured in orbit by measuring the effect of thrust from a pair of PPTs on the spacecraft spin rate.[102] The PPTs were oriented with the thrust vector at 39 deg to the radius vector. This method requires accurate knowledge of the satellite moment of inertia.

7) A simple pendulum thrust stand was developed[103] at Tohoku University and the University of Tokyo, with a 500-μN resolution. The resolution of this type of stand is limited by friction in the pendulum support bearings.

8) A University of Illinois thrust stand[6] with a 50-kg capacity and a sensitivity of <10 μN uses a James Watt straightline steam engine linkage invented in 1784. The design uses eight flexural pivots and an LVDT displacement sensor, and employs a calibration system developed by Haag at NASA.[99] The long period of the system, up to 30 s, isolates the platform from outside mechanical disturbances. Vertical displacement of the c.m. is as small as 10^{-10} m.

Acknowledgments

The authors wish to acknowledge F. Curran and E. Pencil of the NASA Lewis Research Center, M. Birkan of the U.S. Air Force Office of Scientific Research, and R. Spores of the U.S. Air Force Research Laboratory for continued support and collaboration on PPT research. They are indebted to R. Vondra and N. Antropov, and to V. Khrabrov, developer of the first Russian erosion PPT, for making information available on the PPT flown on Zond-2. They are also grateful for information supplied by G. Spanjers of the U.S. Air Force Research Laboratory and M. Wilson of Primex Aerospace Company. R. L. Burton wishes to thank P. Rustan, Office of the Secretary of the U.S. Air Force, and M. Osborn and P. Lynn of the U.S. Naval Research Laboratory for support on PPT development. P. J. Turchi acknowledges U.S. Air Force Office of Scientific Research for its support of the development of equation-of-state and transport properties of molecular plasmas, and the Ohio Supercomputer Center, Columbus, Ohio, for support of numerical computations. He expresses his gratitude to R. E. Peterkin Jr., for continued assistance with the MACH2 code, and to P. G. Mikellides for collaboration on PPT simulations.

References

[1]Guman, W. J., and Williams, T. E., "Pulsed Plasma Microthruster for Synchronous Meteorological Satellite (SMS)," AIAA Paper 73-1066, Nov. 1973.

[2]Ebert, W. L., Kowal, S. J., and Sloan, R. F., "Operational Nova Spacecraft Teflon Pulsed Plasma Thruster System," AIAA Paper 89-2497, July 1989.

[3]Kowal, S. J. (ed.), *Post-Launch Results of the TIP Spacecraft Pulsed-Plasma Microthrusters*, Vol. 5, Applied Physics Lab., Monterey, CA, 1980.

[4]Brill, Y., Eisner, A., and Osborn, L., "The Flight Application of a Pulsed Plasma Microthruster; The Nova Satellite," AIAA Paper 82-1956, July 1982.

[5]Guman, W. J., and Nathanson, D. M., "Pulsed Plasma Microthruster Propulsion System for Synchronous Orbit Satellite," *Journal of Spacecraft and Rockets*, Vol. 7, No. 4, 1970, pp. 409–415.

[6]Vondra, R. J., and Thomassen, K. I., "Flight Qualified Pulsed Electric Thruster for Satellite Control," *Journal of Spacecraft and Rockets*, Vol. 11, No. 9, 1974, pp. 613–617; also AIAA Paper 73-1067, Oct. 1973.

[7]Vondra, R. J., "The MIT Lincoln Laboratory Pulsed Plasma Thruster—A Final Report on the LES-8/9 Pulsed Plasma Thruster," AIAA Paper 76-998, Nov. 1976.

[8]LaRocca, A. V., "Pulsed Plasma Thruster System for Attitude and

Station Control of Spacecraft," *First Western Space Congress*, 1970, pp. 688–702.

[9]Akimov, V., Nagel, I., Ogloblina, I., Antropov, N., Pokryshkin, A., Popov, G., and Rudikov, A., "Analysis of PPT Potentialities in Solving the Satellite Orbit Control Tasks," 25th International Electric Propulsion Conf., Paper 97-146, Aug. 1997.

[10]Janson, S. W., "The On-Orbit Role of Electric Propulsion," AIAA Paper 93-2220, June 1993.

[11]Meckel, N. J., Cassady, R. J., Osborne, R. D., Hoskins, W. A., and Myers, R. M., "Investigation of Pulsed Plasma Thrusters for Spacecraft Attitude Control," 25th International Electric Propulsion Conf., Paper 97-128, Aug. 1997.

[12]Cassady, R. J., Meckel, N. J., Hoskins, W. A., Myers, R. M., Oleson, S. R., and McGuire, M., "Pulsed Plasma Thruster Systems for Spacecraft Attitude Control," 10th AIAA/Utah State University Conference on Small Satellites, Sept. 1996.

[13]Christensen, J., Freick, K., Hart, S., Norenberg, K., Haag, T., Patterson, M., Rawlin, V., Sovey, J., Anderson, J., Becker, R., and Polk, J., "Design and Fabrication of a 2.3 kW Ion Thruster for the Deep Space 1 Mission," AIAA Paper 98-3327, July 1998.

[14]Blandino, J. J., Cassady, R. J., and Peterson, T. T., "Pulsed Plasma Thrusters for the New Millennium Interferometer (DS-3) Mission," 25th International Electric Propulsion Conf., Paper 97-192, Aug. 1997.

[15]Jahn, R. G., *Physics of Electric Propulsion*, McGraw–Hill, New York, 1968.

[16]Turchi, P. J., "Electric Rocket Propulsion Systems," *Space Propulsion Analysis and Design*, 1st ed., Vol. 1, McGraw–Hill, New York, 1995.

[17]Guman, W. J., and Peko, P. E., "Solid-Propellant Pulsed Plasma Microthruster Studies," *Journal of Spacecraft and Rockets*, Vol. 6, No. 6, 1968, pp. 732, 733; also AIAA Paper 68-85, Jan. 1968.

[18]Vondra, R. J., and Thomassen, K. I., "Performance Improvements in Solid Fuel Microthrusters," *Journal of Spacecraft and Rockets*, Vol. 9, No. 10, 1972, pp. 738–742; also AIAA Paper 72-210, Jan. 1972.

[19]Andrenucci, M., Lensi, R., Naso, V., and Melli, R., "Design of Solid-Propellant MPD Thrusters," *Electric Propulsion and Its Application to Space Missions*, edited by R. C. Fincke, Vol. 79, Progress in Astronautics and Aeronautics, IAA, New York, 1980, pp. 586–601.

[20]Palumbo, D. J., and Guman, W. J., "Continuing Development of the Short-Pulsed Ablative Space Propulsion System," AIAA Paper 72-1154, Nov. 1972.

[21]Shapiro, A. H., "The Dynamics and Thermodynamics of Compressible Fluid Flow," Ronald, New York, 1953.

[22]Ruchti, C. B., and Niemeyer, L., "Ablation Controlled Arcs," *IEEE Transactions on Plasma Science*, Vol. PS-14, No. 4, 1986, pp. 423–434; also IEEE Log 8609592, Aug. 1986.

[23]Wentink, T., Jr., "High Temperature Behavior of Teflon," AVCO–Everett Research Laboratory, AF04(647)-278, Everett, MA, July 1959.

[24]Turchi, P. J., "Directions for Improving PPT Performance," *Proceedings of the 25th International Electric Propulsion Conference*, Vol. 1, Electric Rocket Propulsion Society, Worthington, OH, 1998, pp. 251–258.

[25]Guman, W. J., "Pulsed Plasma Technology in Microthrusters," Fairchild Hiller Corp., Farmingdale, NY, AFAPL-TR-68-132, Nov. 1968.

[26]Spanjers, G. G., Lotspeich, J. S., McFall, K. A., and Spores, R. A., "Propellant Losses Because of Particulate Emission in a Pulsed Plasma Thruster," *Journal of Propulsion and Power*, Vol. 14, No. 4, 1998, pp. 554–559.

[27]Marshall, J., "Performance of a Hydromagnetic Plasma Gun," *Physics of Fluids*, Vol. 3, No. 1, 1960, pp. 134, 135.

[28]Burton, R. L., and Chang, O., Y.-S., "Acceleration Process in a Stabilized High-Current Arc," *AIAA Journal*, Vol. 6, No. 11, 1968, pp. 2190–2192.

[29]Ziemer, J. K., Choueiri, E., and Birx, D., "Trends in Performance Improvements of a Gas-Fed Pulsed Plasma Thruster," Paper 97-040, 25th International Electric Propulsion Conf., Paper 97-040, Aug. 1997.

[30]Larson, A. V., Gooding, T., Hayworth, B. and Ashby, D., "An Energy Inventory in a Coaxial Plasma Accelerator Driven by a Pulse Line Energy Source," *AIAA Journal*, Vol. 3, No. 5, 1965, pp. 977–979.

[31]Aronowitz, L., and Duclos, D. P. (ed.), *Characteristics of the Pinch Discharge in a Pulsed Plasma Accelerator*, Vol. 9, Academic, New York, 1963.

[32]Burton, R. L., "Acceleration of Plasma by a Propagating Current Sheet," *Physics of Fluids*, Vol. 11, No. 6, 1968, pp. 1231–1237.

[33]Burton, R. L., and Tiliakos, N., "Injected Propellant Ionization in MPD Thrusters," *Journal of Propulsion and Power*, Vol. 9, No. 5, 1993, pp. 764–770.

[34]Tiliakos, N., "A Theoretical Study of Propellant Preionization in Self-field Magnetoplasmadynamic Thrusters," M.S. Thesis, Univ. of Illinois at Urbana–Champaign, IL, 1993.

[35]Burton, R. L., Clark, K. E., and Jahn, R. G., "Measured Performance of a Multimegawatt MPD Thruster," *Journal of Spacecraft*, Vol. 20, No. 3, 1983, pp. 299–304.

[36]Cheng, D. Y., "Application of a Deflagration Plasma Gun as a Space Propulsion Thruster," *AIAA Journal*, Vol. 9, No. 9, 1971, pp. 1681–1685.

[37]Glushko, V. P., "Methods in Rocket Engineering," *Academy of Sciences USSR*, 1977.

[38]Ashby, D. E. T. F., "Quasi-Steady-State Pulsed Plasma Thrusters," *AIAA Journal*, Vol. 4, No. 5, 1966, pp. 831–835.

[39]LaRocca, A. V., *Semisolid Propellant and Thruster Therefor*, U.S. Patent No. 3,575,003, 1971.

[40]Vondra, R. J., "One Millipound Pulsed Plasma Thruster Development," AIAA Paper 82-1877, Nov. 1982.

[41]Palumbo, D. J., and Guman, W. J., "Effects of Propellant and Electrode Geometry on Pulsed Ablative Plasma Thruster Performance," AIAA Paper 75-409, March 1975.

[42]An, S.-M., Wu, H.-J., Feng, X.-Z., and Liu, W.-X., "Space Flight Test of Electric Thruster System MDT-2A," *Journal of Spacecraft and Rockets*, Vol. 21, No. 6, 1984, pp. 593–594; also AIAA Paper 82-1874, Nov. 1982.

[43]Paccani, G., "A Coaxial, Nonsteady, Solid Propellant, MPD Thruster Experimental Analysis," AIAA Paper 87-1095, May 1987.

[44]Paccani, G., "Experimental Analysis of a Coaxial MPD Thruster with Segmented Anodes," *Proceedings of the 23rd International Electric Propulsion Conference*, Electric Rocket Propulsion Society, Worthington, OH, 1995.

[45]Kimura, I., Ogiwara, K., Takegahara, H., and Suzuki, Y., "Effect of Applied Magnetic Fields on a Solid-Propellant Pulsed Plasma Thruster," AIAA Paper 79-2098, Oct. 1979.

[46]Takegahara, H., Ohtsuka, T., and Kimura, I., "Effect of Applied Magnetic Fields on a Solid-Propellant Pulsed Plasma Thruster," 17th International Electric Propulsion Conf., Paper 84-50, May 1984.

[47]Hirata, M., and Murakami, H., "Exhaust Gas Analysis of a Pulsed Plasma Engine," AIAA Paper 84-52, May 1984.

[48]Yuan-Zhu, K., "Effects of Propellant Geometry on PPT Performance," AIAA Paper 84-94, May 1984.

[49]Turchi, P. J., "An Electric Propulsion Development Strategy Based on the Pulsed Plasma Microthruster," AIAA Paper 82-1901, Nov. 1982.

[50]Turchi, P. J., "Strategy for Electric Propulsion Development—Basic Research Needs," *Orbit-Raising and Maneuvering Propulsion*, edited by L. H. Caveny, Vol. 89, Progress in Astronautics and Aeronautics, AIAA, New York, 1984, pp. 233–240.

[51]Turchi, P. J., Boyer, C. N., and Davis, J. F., "Multi-Stage Plasma Propulsion," AIAA Paper 84-51, May 1984.

[52]Deininger, W. D., and Vondra, R. J., "Design and Performance of an Arcjet Nuclear Electric Propulsion System for a Mid-1990's Reference Mission," AIAA Paper 87-1037, May 1987.

[53]Myers, R. M., Oleson, S. R., McGuire, M., Meckel, N. J., and Cassady, R. J., "Pulsed Plasma Thruster Technology for Small Satellite Missions," 9th AIAA/Utah State University Conf. on Small Satellites, Sept. 1995; also NASA CR-1984271995, Sept. 1995.

[54]Myers, R. M., "Electromagnetic Propulsion for Spacecraft," AIAA Paper 93-1086, Feb. 1993.

[55]Solbes, A., and Vondra, R. J., "Performance Study of a Solid Fuel-Pulsed Electric Microthruster," *Journal of Spacecraft and Rockets*, Vol. 10, No. 6, 1973, pp. 406–410; also AIAA Paper 72-458, April 1972.

[56]Antropov, N. N., Krivonosov, I. G., Popov, G. A., and Rudikov, A. I., "PPT Model Experimental Refinement," AIAA Paper 96-2728, July 1996.

[57]Antropov, N., Gomilka, L., Diakonov, G., Krivonosov, I., Popov, G., and Orlov, M., "Parameters of Plasmoids Injected by PPT," AIAA Paper 97-2921, July 1997.

[58]Kimura, I., Yanagi, R., and Inoue, S., "Preliminary Experiments on Pulsed Plasma Thrusters with Applied Magnetic Fields," AIAA/DGLR 13th International Electric Propulsion Conf., Paper 78-655, April 1978.

[59]Palumbo, D. J., and Guman, W. J., "Propellant Sidefeed-Short Pulse Discharge Thruster Studies," Fairchild Industries, Inc., N72-20756, Farmingdale, NY, Jan. 1972.

[60]Guman, W. J., "Designing Solid Propellant Pulsed Plasma Thrust-

ers,'' AIAA Paper 75-410, March 1975.
[61]Palumbo, D. J., and Guman, W. J., ''Pulsed Plasma Propulsion Technology,'' Fairchild Industries, Inc., AD-768224, Sept. 1973.
[62]Arrington, L. A., Haag, T. W., Pencil, E. J., and Meckel, N. J., ''A Performance Comparison of Pulsed Plasma Thruster Electrode Configurations,'' 25th International Electric Propulsion Conf., IEPC Paper 97-127, Aug. 1997.
[63]Alexeev, Y. A., and Kazeev, M. N., ''High Power Ablative Pulsed Plasma Thruster for Technology Applications,'' 25th International Electric Propulsion Conf., Paper 97-165, Aug. 1998.
[64]Burton, R. L., Fleischer, D., Goldstein, S. A., and Tidman, D. A., ''Experiments on a Repetitively Pulsed Electrothermal Thruster,'' *Journal of Propulsion and Power*, Vol. 6, No. 2, 1990, pp. 139–144; also AIAA Paper 87-1043, May 1987.
[65]Willmes, G. F., ''A Low Power Pulsed Arcjet Thruster for Spacecraft Propulsion,'' Ph.D. Dissertation, Univ. of Illinois at Urbana–Champaign, IL, 1997.
[66]Wilson, M. J., Bushman, S. S., and Burton, R. L., ''A Compact Thrust Stand for Pulsed Plasma Thrusters,'' 25th International Electric Propulsion Conf., Paper 97-122, Aug. 1997.
[67]Burton, R. L., Bushman, S. S., and Antonsen, E. L., ''Arc Measurements and Performance Characteristics of a Coaxial Pulsed Plasma Thruster,'' AIAA Paper 98-3660, July 1998.
[68]Leiweke, R. J., Turchi, P. J., Kamhawi, H., and Myers, R. M., ''Experiments with Multi-Material Propellants in Ablation-Fed Pulsed Plasma Thrusters,'' AIAA Paper 95-2916, July 1995.
[69]Palumbo, D. J., and Guman, W. J., ''Effects of Propellant and Electrode Geometry on Pulsed Ablative Plasma Thruster Performance,'' *Journal of Spacecraft and Rockets*, Vol. 13, No. 3, 1976, pp. 163–167; also AIAA Paper 75-409, March 1975.
[70]Spanjers, G. G., Malak, J. B., Leiweke, R. J., and Spores, R. A., ''The Effect of Propellant Temperature on Efficiency in a Pulsed Plasma Thruster,'' AIAA Paper 97-2920, July 1997.
[71]Kamhawi, H., and Turchi, P. J., ''PPT Thermal Management,'' *Proceedings of the 25th International Electric Propulsion Conference*, Vol. 1, Electric Rocket Propulsion Society, Worthington, OH, 1998, pp. 789–796.
[72]Kamhawi, H., Turchi, P. J., Leiweke, R. J., and Myers, R. M., ''Design and Operation of a Laboratory Benchmark PPT,'' AIAA Paper 96-2732, July 1996.
[73]Roy, R. I. S., Hastings, D. E., and Gatsonis, N. A., ''A Review of Contamination from Electric Propulsion Thrusters,'' AIAA Paper 94-2469, June 1994.
[74]Rudolph, L. K., and Jones, R. M., ''Pulsed Plasma Thruster Contamination Studies,'' AIAA Paper 79-2106, Oct. 1979.
[75]Myers, R. M., Arrington, L. A., Pencil, E. J., Carter, J., Heminger, J., and Gatsonis, N., ''Pulsed Plasma Thruster Contamination,'' AIAA Paper 96-2729, July 1996.
[76]Vondra, R., Thomassen, K., and Solbes, A., ''A Pulsed Electric Thruster for Satellite Control,'' *Proceedings of the IEEE*, Vol. 59, No. 2, 1971, pp. 271–277.
[77]Guman, W. J., Vondra, R. J., and Thomassen, K., ''Pulsed Plasma Propulsion System Studies,'' AIAA Paper 70-1148, Aug. 1970.
[78]Thomassen, K. I., and Vondra, R. J., ''Exhaust Velocity Studies of a Solid Teflon Pulsed Plasma Thruster,'' *Journal of Spacecraft and Rockets*, Vol. 9, No. 1, 1972, pp. 61–64.
[79]Thomassen, K. I., and Tong, D., ''Interferometric Density Measurements in the Arc of a Pulsed Plasma Thruster,'' *Journal of Spacecraft and Rockets*, Vol. 10, No. 3, 1973, pp. 163, 164; also AIAA Paper 72-463, April 1972.
[80]Hirata, M., Murakami, H., Ono, M., and Nakamaru, K., ''A Space Test of a Pulsed Plasma Engine,'' *Proceedings of the 13th International Symposium of Space Technology and Science*, Tokyo, Japan, 1982, pp. 109–116.
[81]Spanjers, G. G., McFall, K. A., III, and Spores, R. A., ''Investigation of Propellant Inefficiencies in a Pulsed Plasma Thruster,'' AIAA Paper 96-2723, July 1996.
[82]Markusic, T. E., and Spores, R. A., ''Spectroscopic Emission Measurements of a Pulsed Plasma Thruster Plume,'' AIAA Paper 97-2924, July 1997.
[83]Eckman, R., Gatsonis, N., Myers, R., and Pencil, E., ''Experimental Investigation of the LES 8/9 Pulsed Plasma Thruster Plume,'' 25th International Electric Propulsion Conf., IEPC Paper 97-126, Aug. 1997.
[84]Turchi, P. J., and Mikellides, R. G., ''Modeling of Ablation-Fed Pulsed Plasma Thrusters,'' AIAA Paper 95-2915, June 1995.
[85]Palumbo, D. J., and Begun, M., ''Plasma Acceleration in Pulsed Ablative Arc Discharges: Final Report for Period 15 March 1974–31 March 1977,'' Fairchild Republic Co., F44620-74-C-0055, April 1977.
[86]Turchi, P. J., et al., ''Generation of High Energy X-Radiation Using a Plasma Flow Switch,'' *Journal of Applied Physics*, Vol. 69, No. 4, 1991, pp. 1999–2005.
[87]Turchi, P. J., Davis, J. F., and Roderick, N. F., ''MPD Arcjet Thrust Chamber Flow Studies,'' AIAA Paper 90-2664, July 1990.
[88]Mikellides, P. G., Turchi, P. J., and Roderick, N. F., ''Analysis of Applied-Field Plasma Thrusters Using the MACH2 Code,'' AIAA Paper 94-3338, July 1994.
[89]Mikellides, P. G., and Turchi, P. J., ''Modeling of Late-Time Ablation in Teflon Pulsed Plasma Thrusters,'' AIAA Paper 96-2733, July 1996.
[90]Cranfill, C. W., ''EOSPAC:A Subroutine Package for Accessing the Los Alamos Data Library,'' Los Alamos National Lab., LA-9728-M, Los Alamos, NM, Aug. 1983.
[91]Schmahl, C. S., and Turchi, P. J., ''Development of Equation-of-State and Transport Properties for Molecular Plasmas in Pulsed Plasma Thrusters Part I: A Two-Temperature Equation-of-State for Teflon,'' *Proceedings of the 25th International Electric Propulsion Conference*, Vol. 1, Electric Rocket Propulsion Society, Worthington, OH, 1998, pp. 781–788.
[92]Yin, X., and Gatsonis, N., ''Numerical Investigation of Pulsed Plasma Thruster Plumes,'' 25th International Electric Propulsion Conf., IEPC Paper 97-036, Aug. 1997.
[93]Turchi, P. J., Leiweke, R. J., and Kamhawi, H., ''Design of an Inductively-Driven Pulsed Plasma Thruster,'' AIAA Paper 96-2731, July 1996.
[94]Anderson, H. L. (ed.), *Physics Vade Mecum*, American Institute of Physics, New York, 1981.
[95]Kerrisk, J. F., ''Current Distribution and Inductance Calculations for Rail-Gun Conductors,'' Los Alamos National Lab., LA-9092-MS, Los Alamos, NM, 1981.
[96]Burton, R. L., Wilson, M. J., and Bushman, S. S., ''Energy Balance and Efficiency of the Pulsed Plasma Thruster,'' AIAA Paper 98-3808, July 1998.
[97]Cubbin, E. A., Ziemer, J. K., Choueiri, E. Y., and Jahn, R. G., ''Laser Interferometry for Pulsed Plasma Thruster Performance Measurement,'' 24th International Electric Propulsion Conf., IEPC Paper 95-195, Sept. 1995.
[98]Haag, T. W., ''Thrust Stand for High-Power Electric Propulsion Devices,'' *Review of Scientific Instruments*, Vol. 62, No. 5, 1991, pp. 1186–1191.
[99]Haag, T. W., ''PPT Thrust Stand,'' AIAA Paper 95-2917, July 1995; also NASA TM 107066, July 1995.
[100]Burton, R. L., Goldstein, S. A., Hilko, B. K., Tidman, D. A., and Winsar, N. K., ''Investigation of a Pulsed Electrothermal Thruster System,'' NASA CR-174768, April 1984.
[101]Stark, K. W., Dennis, T., McHugh, D., and Williams, T., ''Design and Development of a Micropound Extended Range Thrust Stand (MERTS),'' NASA Goddard Space Flight Center, Greenbelt, MD, Aug. 1971.
[102]Hirata, M., and Murakami, H., ''Impulse Measurements of a Pulsed-Plasma Engine on Engineering Test Satellite-IV,'' *Journal of Spacecraft and Rockets*, Vol. 21, No. 6, 1984, pp. 553–557; also AIAA Paper 82-1875, Nov. 1982.
[103]Sasoh, A., and Arakawa, Y., ''A High-Resolution Thrust Stand for Ground Tests of Low-Thrust Space Propulsion Devices,'' *Review of Scientific Instruments*, Vol. 64, No. 3, 1993, pp. 719–723.